Streaming potential measurements: 1. Properties of the electrical double layer from crushed rock samples

Benoit Lorne, Frédéric Perrier, Jean-Philippe Avouac

JOURNAL OF GEOPHYSICAL RESEARCH, VOL. 104, NO. B8, PAGES 17,857–17,877, AUGUST 10, 1999

Streaming potential measurements 1. Properties of the electrical double layer from crushed rock samples

Benoit Lorne, Frédéric Perrier, and Jean-Philippe Avouac

Commissariat à l'Énergie Atomique, Laboratoire de Détection et de Géophysique, Bruyères-le-Châtel, France

Abstract. The ζ potential has been inferred from streaming potential measurements with crushed rock samples as a function of pH and electrolyte concentration for various salts. The value obtained for crushed Fontainebleau sandstone at pH = 5.7 and a KCl solution with a resistivity of 400 Ω m is -40 ± 5 mV, where the error is dominated by sample to sample variations. The sensitivity of the ζ potential to the electrolyte resistivity for KCl is given experimentally by $\rho_f^{0.23 \pm 0.014}$, where ρ_f is the electrolyte resistivity. The point of zero charge (pzc) is observed for pH = 2.5 ± 0.1, and the ζ potential is positive for pH < pzc and negative for pH > pzc. For pH > 5 the variations of the ζ potential with pH can be approximated by $\zeta(\text{pH})/\zeta(5.7) = 1 + (0.068 \pm 0.004)(\text{pH} - 5.7)$ for $\rho_f = 100$ Ω m. The ζ potential has been observed to be sensitive to the valence of the ions and is approximately reduced by the charge of the cation, unless specific adsorption takes place like in the case of Al^{3+}. The experimental results are well accounted for by a three-layer numerical model of the electrical double layer, and the parameters of this model can be evaluated from the experimental data. The sensitivity of the ζ potential to the rock minerals has also been studied. The ζ potential obtained for granitic rocks is comparable to that obtained for Fontainebleau sandstone but can be reduced by a factor of 2–4 for sandstones containing significant fractions of carbonates or clay. To take into account the effect of the chemical composition of the electrolyte, a chemical efficiency is defined as the ratio of the ζ potential to the ζ potential measured for KCl. This chemical efficiency is measured to be ~80% for typical groundwater but can be as low as 40% for a water with a high dissolved carbonate content. The set of empirical laws derived from our measurements can be used to assess the magnitude of the streaming potentials expected in natural geophysical systems.

1. Introduction

Variations in space and time of the electrical spontaneous potential (SP) have been observed to be associated with geothermal fields [e.g., *Zohdy et al.*, 1973; *Corwin and Hoover*, 1979] and volcanic activity [e.g., *Massenet and Pham*, 1985a; *Zlotnicki and Le Mouël*, 1988; *Fujinawa et al.*, 1992; *Malengreau et al.*, 1994; *Zlotnicki et al.*, 1994; *Hashimoto and Tanaka*, 1995; *Michel and Zlotnicki*, 1998]. Some examples of SP variations with timescales ranging from 1 min to several months, although sometimes controversial, have been reported before earthquakes [*Park et al.*, 1993]. Electric potential variations are also observed at smaller scales, for example, in mountainous areas where they have been found to be associated with topography and the discharge of aquifers [*Ernstson and Scherer*, 1986]. Changes in SP have also been found to be associated with a change in mechanical stress and the collapse of pillars in experiments performed in underground quarries in France [*Morat and Le Mouël*, 1989, 1992].

Although mechanisms like the piezoelectric effect are also advocated [*Yoshida et al.*, 1997], the electrokinetic effect (EKE) is proposed as the most likely mechanism for the generation of these electric potential variations [*Mizutani et al.*, 1976; *Massenet and Pham*, 1985a; *Zlotnicki and Le Mouël*, 1990; *Bernard*, 1992; *Fenoglio et al.*, 1995]. The EKE is the production of electric potentials (called streaming potentials) by fluid motions which are present, for example, in geothermal and volcanic areas. There is also evidence that the seismic cycle involves fluid circulation. *Muir-Wood and King* [1993] have reported large increases of river water discharge in the months following large earthquakes. They infer that mobile water pervades the whole of the upper crust (down to depth of ~10 km) and may be released to the surface during postseismic relaxation. This interpretation is consistent with the suggestion that fluid motion may control the characteristic time associated with aftershock decay [*Nur and Booker*, 1972]. In addition, the apparent low friction on major faults such as the San Andreas fault [e.g., *Byerlee*, 1990], and some aspects of the seismic cycle [e.g., *Sleep and Blanpied*, 1992; *Johnson and McEvilly*, 1995] support the presence in fault zones of fluids that may reach lithostatic pressures. Diffusion of fluids into dilatant zones may also be a significant phenomenon before earthquakes [*Scholz et al.*, 1973]. There is therefore a possibility that shallow or crustal fluids are involved, through the EKE, in the generation of SP variations before earthquakes.

Some experiments have been implemented in order to investigate the role of the EKE in the field [e.g., *Bogoslovsky and Ogilvy*, 1970; *Morat and Le Mouël*, 1992; *Pisarenko et al.*, 1996; *Perrier et al.*, 1998, 1999; *Trique et al.*, 1999]. These investigations require a better understanding of the physics of the EKE

Paper number 1999JB900156.
0148-0227/99/1999JB900156$09.00

at the level of the rock-fluid interface and then at the level of the rock sample. Early laboratory measurements of streaming potentials for geophysical applications were carried out with sand and glass plates [*Ahmad*, 1964; *Ogilvy et al.*, 1969; *Bogoslovsky and Ogilvy*, 1972]. More precise measurements with crushed rock samples were undertaken as a function of pH and temperature [*Ishido and Mizutani*, 1981; *Massenet and Pham*, 1985b; *Morgan et al.*, 1989]. These studies showed that the model of the electrical double layer (EDL), developed by electrochemists for glass capillaries [*Overbeek*, 1960], was valid for rock water systems, with ζ potentials ranging from a few tens of mV to >100 mV. Measurements with intact rock samples were performed by *Jouniaux and Pozzi* [1995a, b, 1997] in a triaxial device, and the effect of deformation and rupture was studied.

These pioneering laboratory studies have left some open questions. The ζ potentials reported by the various authors are often quite different, and discrepancies are also present within the same rock type in a given work [*Jouniaux and Pozzi*, 1995b]. These discrepancies could be due to the experimental procedure or to uncertainties in the electrolyte composition or the pH. Also, although the effect of pH was compared with the predictions of the EDL by *Ishido and Mizutani* [1981], a precise quantitative evaluation of the dependence of the ζ potential upon the fluid resistivity with crushed rocks is not available. A detailed comparison of a consistent set of experimental data, both as a function of electrolyte conductivity and pH, with the predictions of a complete theory of the electrical double layer [*Davis et al.*, 1978] is therefore required. Improving our understanding of the EDL model is also important to address the question of surface electrical conduction in porous media [*Revil and Glover*, 1997].

For this purpose, new streaming potential measurements with a careful monitoring of pH and water composition were undertaken, and their results are reported in this paper, together with a comparison with the predictions of a three-layer theory of the EDL implemented as a complete numerical model valid for any electrolyte composition. Also, various rock-electrolyte interface combinations were studied in order to translate the measurements performed in the laboratory to the chemical conditions of a real geophysical environment.

Some aspects of the physics of the streaming potentials in rock samples are not addressed in this work. Two-phase effects [*Antraygues and Aubert*, 1993; *Sprunt et al.*, 1994] are important in geothermal and volcanic areas, as well as temperature effects [*Somasundaran and Kulkarni*, 1973]. The frequency dependence [*Chandler*, 1981] is also important in relation with electroseismic effects [*Pride and Morgan*, 1991; *Pride*, 1994]. Also, only aqueous electrolytes are considered in this paper, although there might be important applications of the EKE for hydrocarbon reservoirs [*Wurmstich and Morgan*, 1994]. Other questions related to the EKE in rocks, and in particular the permeability dependence, are the subject of a separate companion paper presenting measurements of streaming potentials in rocks during deformation [*Lorne et al.*, this issue].

2. Electrochemistry of the Electrical Double Layer

2.1. General Features of the EDL

The EKE results from the electrical structure of the rock-electrolyte interface. The currently accepted model of this interface is the EDL model of Stern [*Bard and Faulkner*, 1980; *Iler*, 1979; *Overbeek*, 1960], developed from the measurements of electrode potentials and capacities and from streaming potential and electro-osmosis experiments using glass capillaries. A schematic diagram of the rock-fluid interface in the framework of the EDL model is given in Figure 1. Chemical reactions take place between the minerals and the water and salt molecules and result in a net electrical charge at the mineral surface [e.g., *Iler*, 1979; *Glover et al.*, 1994]. Water and salt molecules bound to the rock surface constitute the Helmholtz or Stern layer, which is sometimes divided into inner Helmholtz plane (IHP) and outer Helmholtz plane (OHP). In the IHP, salt and water molecules are directly bound to the mineral structure. In the OHP, solvated salts are more weakly bound to the mineral structure through higher-order interactions. Ions in the electrolyte are affected by this electrical structure in a volume called the diffuse layer (DL), which by definition starts at a plane called the Stern plane. Far from the mineral surface the electrolyte can be considered to be unaffected and is called the free electrolyte. The charge densities in the DL are constrained by the surface charge density in the Stern layer. The most simple theory of the EDL consists in neglecting the width of the Stern layer and to model its charge density by a surface charge density Q_S concentrated on the Stern plane. In this paper, as the spatial structure of the Stern layer has observable consequences, we will use the three-layer theory formulated by *Davis et al.* [1978].

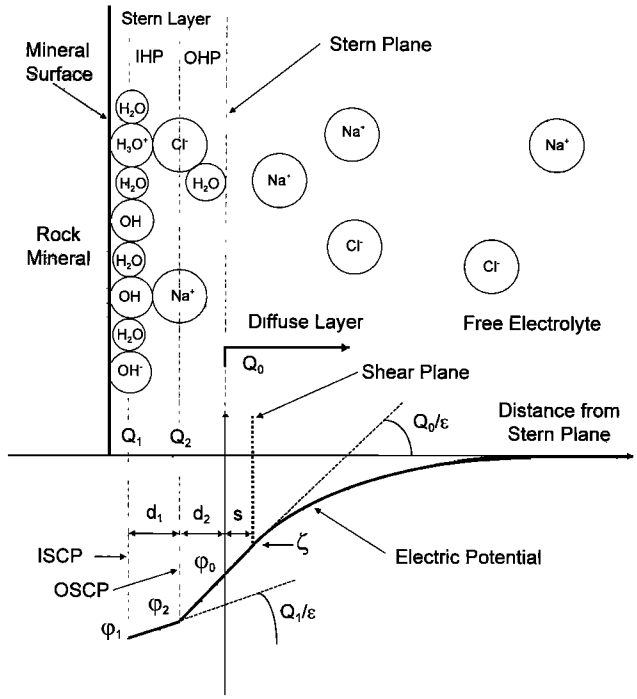

Figure 1. A sketch of the structure of the electrical double layer in the three-layer model (adapted from *Davis et al.* [1978]). IHP, internal Helmholtz plane; OHP, outer Helmholtz plane; ISCP, internal surface charge plane; OSCP, outer surface charge plane. The ζ potential is defined as the electric potential at shear plane, located at a distance s from the Stern plane.

The main equations relating the electric potential to the ionic concentrations and the surface charge density Q_S are recalled. We follow the notations of *Revil and Glover* [1997],

using the theory of *Davis et al.* [1978] and rewriting some equations for implementation in a numerical model.

In order to avoid complications unnecessary for this paper we derive the EDL equations assuming that the macroscopic external electric field is zero. The concentration of ion i in the electrolyte is denoted by c_i, and its electric charge is denoted by $z_i e$ (positive or negative), where e is the fundamentally constant unit electric charge ($e > 0$). The concentrations throughout this paper are expressed in mmol/L. Because the pore dimensions are large compared with the size of the DL, the curvature of the mineral surface will not be taken into account for the electromagnetic problem, and the concentrations depend only on the distance x perpendicular to the Stern plane [*Pride and Morgan*, 1991]. The origin of the x axis is taken on the Stern plane.

2.2. Description of the Rock-Electrolyte Interaction

In the case of quartz the interaction of the mineral surface with an aqueous electrolyte involves the protonation and the deprotonation of the silanol groups [e.g., *Iler*, 1979; *Glover et al.*, 1994; *Revil and Glover*, 1997]

$$\mathrm{Si-O^- + H^+ \overset{K_-}{\longleftrightarrow} Si-OH}, \tag{1}$$

$$\mathrm{Si-OH + H^+ \overset{K_+}{\longleftrightarrow} Si-OH_2^+}, \tag{2}$$

where K_+ and K_- are the equilibrium constants. A surface charge density Q_1 on the rock mineral results from these reactions (Figure 1). This surface charge density depends on the concentration of H^+ ions. Neglecting for the moment the adsorption of other ions, one can define a pH of zero charge (pzc), for which $Q_1 = 0$ (isoelectric point). It is related to the equilibrium constants K_+ and K_- by [*Glover et al.*, 1994]

$$\mathrm{pzc} = -\tfrac{1}{2}\log\frac{K_+}{K_-} = \frac{pK_- - pK_+}{2} \approx 3. \tag{3}$$

For pH larger than pzc the surface will be dominated by $Si - O^-$ sites, and it will develop a net negative charge.

However, this simple picture is complicated by the fact that other ions from the electrolyte also participate in the surface adsorption (Figure 1). For example, for a salt MA the following chemical reactions have to be considered [*Davis et al.*, 1978]:

$$\mathrm{Si-OH + M^+ \overset{K_M}{\longleftrightarrow} Si-OM + H^+}, \tag{4}$$

$$\mathrm{Si-OH + A^- + H^+ \overset{K_A}{\longleftrightarrow} Si-A + H_2O}. \tag{5}$$

Because of the finite size of the ions the adsorption of the M^+ and A^- ions will produce a charge density Q_2 which will be located at a distance d_1 from the plane of charge density Q_1 and at a distance d_2 from the Stern plane (Figure 1). This plane of charge density Q_2 will be referred to as the outer surface charge plane (OSCP) and the plane of charge density Q_1 will be referred to as the inner surface charge plane (ISCP). The representation depicted in Figure 1 will be referred to as the three-layer model of *Davis et al.* [1978]. Even in the case of a complex electrolytic solution (beyond a 1:1 electrolyte), it will be assumed that the charge of the adsorbed ions is located on a single OSCP of charge density Q_2.

The charge densities Q_1 and Q_2 can be written (generalizing equations (18) and (19) of *Davis et al.* [1978])

$$Q_1 = \Gamma_{\mathrm{Si-OH_2^+}} - \Gamma_{\mathrm{Si-O^-}} + \sum_{\mathrm{A}} \Gamma_{\mathrm{Si-A}} - \sum_{\mathrm{M}} \Gamma_{\mathrm{Si-M}}, \tag{6}$$

$$Q_2 = \sum_{\mathrm{M}} \Gamma_{\mathrm{Si-M}} - \sum_{\mathrm{A}} \Gamma_{\mathrm{Si-A}}, \tag{7}$$

where Γ_i is the charge densities of adsorbed species ι per unit surface. The charge densities of the adsorbed species can be expressed in terms of the equilibrium constants and the ionic concentrations [*Davis et al.*, 1978; *Revil and Glover*, 1997]:

$$\Gamma_{\mathrm{Si-OH_2^+}} = \Gamma_{\mathrm{Si-OH}} K_+ c_{\mathrm{H^+}}^{\mathrm{ISCP}}, \tag{8}$$

$$\Gamma_{\mathrm{Si-OH^-}} = \Gamma_{\mathrm{Si-OH}} \frac{K_-}{c_{\mathrm{H^+}}^{\mathrm{ISCP}}}, \tag{9}$$

$$\Gamma_{\mathrm{Si-M}} = \Gamma_{\mathrm{Si-OH}} K_{\mathrm{M}} \frac{c_{\mathrm{M}}^{\mathrm{OSCP}}}{c_{\mathrm{H^+}}^{\mathrm{ISCP}}}, \tag{10}$$

$$\Gamma_{\mathrm{Si-A}} = \Gamma_{\mathrm{Si-OH}} K_{\mathrm{A}} c_{\mathrm{A}}^{\mathrm{OSCP}} c_{\mathrm{H^+}}^{\mathrm{ISCP}}, \tag{11}$$

$$\Gamma_{\mathrm{Si-OH}} = \Gamma_S^0 \frac{1}{1 + K_+ c_{\mathrm{H^+}}^{\mathrm{ISCP}} + \dfrac{K_-}{c_{\mathrm{H^+}}^{\mathrm{ISCP}}} + \displaystyle\sum_{\mathrm{M}} K_{\mathrm{M}} \frac{c_{\mathrm{M}}^{\mathrm{OSCP}}}{c_{\mathrm{H^+}}^{\mathrm{ISCP}}} + \sum_{\mathrm{A}} K_{\mathrm{A}} c_{\mathrm{H^+}}^{\mathrm{ISCP}} c_{\mathrm{A}}^{\mathrm{OSCP}}}, \tag{12}$$

where Γ_S^0 is the total surface charge density:

$$\Gamma_S^0 = \Gamma_{\mathrm{Si-OH}} + \Gamma_{\mathrm{Si-OH_2^+}} + \Gamma_{\mathrm{Si-OH^-}} + \sum_{\mathrm{M}} \Gamma_{\mathrm{Si-M}} + \sum_{\mathrm{A}} \Gamma_{\mathrm{Si-A}}. \tag{13}$$

In general, the concentrations of ions at the ISCP and the OSCP, and thus Q_1 and Q_2 (equations (6) and (7)), depend on the electric potential. Provided the equilibrium constants, the capacitances, and the total site charge density Γ_S^0 are known, the electric potential $\varphi(x)$ can be solved from the concentrations in the free electrolyte.

The total charge density Γ_S^0 is constrained by the lattice parameters of the minerals. The best known interface is the quartz-NaCl interface. Some numerical values can be found in the literature [*Revil and Glover*, 1997; *Ishido and Mizutani*, 1981]. In this paper a value of $\Gamma_S^0 = 1.5\ e/\mathrm{nm}^2$ will be used. *Davis et al.* [1978] suggest a higher value of $\Gamma_S^0 = 5\ e/\mathrm{nm}^2$. For pH > pzc and for most salts the net surface charge on the quartz surface is dominated by $Si - O^-$ groups, and the net surface charge $Q_1 + Q_2$ is negative. The electric potential in the DL is therefore negative, as depicted in Figure 1. In principle, the electric potential in the Stern layer can change sign, but the most simple configuration, as depicted in Figure 1, is one in which the surface charge is dominated by the charge on the ISCP.

Since in this three-layer model the charge distributions are concentrated on two parallel planes, the electric potential in the Stern layer varies linearly between each plane (as illustrated in Figure 1) and is constrained by the boundary conditions

$$\left.\frac{d\varphi}{dx}\right|_1 = -\frac{Q_1}{\varepsilon_S}, \tag{14}$$

$$\left.\frac{d\varphi}{dx}\right|_2 - \left.\frac{d\varphi}{dx}\right|_1 = -\frac{Q_2}{\varepsilon_S}, \tag{15}$$

where ε_S is the permittivity of the Stern layer.

These equations can be rewritten in terms of the potentials φ_0, φ_1, and φ_2 on the Stern plane, the ISCP, and OSCP, respectively [*Davis et al.*, 1978]:

$$\varphi_2 - \varphi_1 = -\frac{Q_1}{C_1}, \tag{16}$$

$$\varphi_0 - \varphi_2 = \frac{Q_0}{C_2}, \tag{17}$$

where the constants C_1 and C_2 are the ISCP and OSCP capacitances, given by $C_1 = \varepsilon_S/d_1$ and $C_2 = \varepsilon_S/d_2$, and Q_0 is the charge density in the diffuse layer. Electroneutrality implies that

$$Q_0 + Q_1 + Q_2 = 0. \tag{18}$$

In general, for quartz, Q_0 is positive.

In this paper the EDL model of *Revil and Glover* [1997] will also be used. In this model the spatial structure of the Stern layer is neglected, and both the ISCP and the OSCP are assumed to coincide with the Stern plane. Then the diffuse layer charge density can be expressed as

$$Q_0 = -\Gamma_S^0 \frac{K_+ c_{H^+} - \dfrac{K_-}{c_{H^+}}}{1 + K_+ c_{H^+} - \dfrac{K_-}{c_{H^+}} + \sum_M K_M \dfrac{c_M}{c_{H^+}} + \sum_A K_A c_A c_{H^+}}, \tag{19}$$

where all concentrations are evaluated at the Stern plane. In this simplified model the charge density also depends on the electric potential and the concentrations in the free electrolyte. In this paper we will discuss the limits of this approximation compared with the three-layer model. The model of *Ishido and Mizutani* [1981], which derives the charge density function from thermodynamics arguments, will also be compared with the data.

The most simple assumption is to assume that the surface charge is constant, as in early models of *Overbeek* [1960]. We will also illustrate in this paper that this simple theory is incompatible with the data.

2.3. Electrical Potential and Ion Distribution in the Diffuse Layer

The electrical potential in the DL is given by the one-dimensional Poisson equation:

$$\frac{d}{dx}\left[\varepsilon(x)\frac{d}{dx}\varphi(x)\right] = -\rho(x), \tag{20}$$

where φ is the electrical potential, ε is the dielectric permittivity of the solution, and ρ is the electric charge density:

$$\rho(x) = F\sum_i z_i c_i(x), \tag{21}$$

where $F = Ne$ is the Faraday charge, N being the Avogadro number.

Neglecting the dielectric saturation, an assumption which is valid if the absolute value of the Stern plane potential is <300 mV [*Pride and Morgan*, 1991], the permittivity can be taken as constant in the DL. Assuming isobaric thermal equilibrium, ionic concentrations can be expressed in terms of the Boltzmann distribution [*Pride and Morgan*, 1991; *Pride*, 1994; *Revil and Glover*, 1997]

$$c_i(x) = c_i^0 \exp\left[-z_i\frac{\varphi(x)}{v_0}\right], \tag{22}$$

where c_i^0 is the ionic concentration in the free electrolyte. The quantity v_0, defined by

$$v_0 = \frac{2kT}{e}, \tag{23}$$

where k is the Boltzmann constant, gives the typical scale of the electric potential. The value of v_0 at 25°C is 51.4 mV.

We will assume that (22) is also valid in the Stern layer [*Davis et al.*, 1978]. The concentrations in the Stern layer are then given by

$$c_{H^+}^{ISCP} = c_{H^+}^0 \exp\left[-2\frac{\varphi_1}{v_0}\right], \tag{24}$$

$$c_M^{OSCP} = c_M^0 \exp\left[-2z_M\frac{\varphi_2}{v_0}\right], \tag{25}$$

$$c_A^{OSCP} = c_A^0 \exp\left[-2z_A\frac{\varphi_2}{v_0}\right]. \tag{26}$$

The densities of adsorbed Si − OH_2^+ and Si − OH^-, to first approximation, are controlled by φ_1 (see equations (8) to (11)), whereas the densities of adsorbed Si − M and Si − A, for monovalent ions, are controlled by the difference $\varphi_2 - \varphi_1$.

To solve the electric potential in the diffuse layer, (22) is combined with (20) and (21) and leads to the Poisson-Boltzmann equation

$$\frac{d^2\varphi}{dx^2} = -\frac{F}{\varepsilon}\sum_i z_i c_i^0 \exp\left[-2z_i\frac{\varphi}{v_0}\right]. \tag{27}$$

A standard method to deal with this equation [e.g., *Bard and Faulkner*, 1980] is to multiply by $d\varphi/dx$ and integrate from $x = 0$ to $x = \infty$, where $d\varphi/dx = 0$. A first-order differential equation for the potential is then derived

$$\frac{d\varphi}{dx} = \text{sign}\,(Q_0)\frac{v_0}{\chi_d}\sqrt{\frac{\sum_i c_i^0\left[\exp\left(-2z_i\dfrac{\varphi}{v_0}\right) - 1\right]}{2\sum_i z_i^2 c_i^0}} \tag{28}$$

The square root is a dimensionless function. The length scale is set by the Debye screening length χ_d defined by [*Bard and Faulkner*, 1980]

$$\chi_d = \sqrt{\frac{\varepsilon kT}{Fe\sum_i z_i^2 c_i^0}} \tag{29}$$

For the solutions considered in this paper the order of magnitude of the Debye length varies between a few nanometer to a few hundred nanometers.

The solution for the electric potential is defined by the boundary condition at the Stern plane

$$\frac{d\varphi}{dx}(x=0) = \frac{Q_0}{\varepsilon}. \tag{30}$$

This condition, combined with (6), (7), (16), (17), and (28), gives a complete set of equations for the potentials φ_0, φ_1, and φ_2. This set of equations can be solved numerically by an iterative zero search algorithm, and the potential in the DL as a function of x can then be obtained using the obtained value for φ_0 and a numerical integration of (28). The electrical structure of the DL can be observed through macroscopic effects such as the surface conductivity or the streaming potential.

2.4. EKE Effect in Capillary Models

The EKE results from the motion of the electrolyte with respect to the rock surface. The electrolyte will be characterized by its composition and concentrations. Its resistivity (conductivity) will be noted ρ_f (σ_f). The sample resistivity (conductivity) will be noted ρ_r (σ_r). In general, the sample conductivity can be written as

$$\sigma_r = \frac{\sigma_f}{F} = \frac{\sigma_f}{F_0} + \sigma_S, \tag{31}$$

where σ_S is the surface conductivity, F is the formation factor, and F_0 is the bulk formation factor. Note that the constant term in (31) can also include additional contributions not related to the electrolyte, such as conductive mineral phases.

Let Δp be the pressure difference across the sample and ΔV be the potential difference between its high- and low-pressure ends, taking the reference point for potential at the high-pressure end [*Morgan et al.*, 1989]. The streaming potential coefficient C_S is defined as

$$C_S = \Delta V/\Delta p. \tag{32}$$

It is the experimentally measured quantity, and it is positive for most quartz-electrolyte interfaces.

In capillary models of porous media the streaming potential coefficient can be related to the electrical structure of the EDL by the Helmholtz-Smoluchowski equation [*Overbeek*, 1960]

$$C_S = -\frac{\varepsilon}{\eta}\zeta\rho_f\frac{F}{F_0}, \tag{33}$$

where η is the dynamic viscosity of the solvent and ζ is the electric potential on the shear plane (Figure 1).

In principle, the shear plane might not coincide with the Stern plane. If s is the distance between the shear plane and the Stern plane, then the value of the ζ potential is defined as

$$\zeta = \varphi(s). \tag{34}$$

The meaning of the distance s is not very clear; however, it might reflect the roughness of the mineral surface, as argued by *Bikerman* [1964]. Several values have been used, varying from 2 nm [*Ishido and Mizutani*, 1981] to 0.2 nm [*Revil and Glover*, 1997]. This point is addressed in the discussion. For most quartz-electrolyte solutions the ζ potential is negative (Figure 1).

The term F/F_0 in (33) is a correction introduced by the presence of surface conductivity [*Overbeek*, 1960; *Jouniaux and Pozzi*, 1995a], and it can be expressed as

$$\frac{F}{F_0} = \frac{1}{1+\rho_f\sigma_S F_0}. \tag{35}$$

In practice, for Fontainebleau sandstone, for example, this ratio is <0.5 only for values of electrolyte resistivity >1000 Ω m, and the correction is negligible (<1%) for all measurements performed with electrolyte resistivity <400 Ω m.

When the surface conductance can be neglected, the streaming potential coefficient is proportional to the electrolyte resistivity in (33), and this fact is an important aspect of the EKE. The order of magnitude of the streaming potential coefficient is $3\rho_f$ mV/0.1 MPa with the electrolyte resistivity ρ_f expressed in Ω m, assuming a ζ potential of −50 mV.

2.5. EKE Effect in Porous Media

In a porous medium the description of the EKE effect is more complicated. It can be shown that the Helmholtz-Smoluchowski equation remains valid in the case of a porous material under rather general assumptions [*Pride*, 1994], using a volume-averaging procedure. However, the Helmholtz-Smoluchowski equation remains to be tested experimentally in detail with real rocks. In particular, the fact that the percolation patterns for the hydraulic problem (flow velocities) and the electrical problem do not necessarily coincide [*David*, 1993] may affect the streaming potential. This problem is discussed in detail by *Lorne et al.* [this issue].

In this paper, where we are concerned with crushed samples, we will assume that the Helmholtz-Smoluchowski equation remains valid. In the following, in order to avoid relying on assumptions on surface conductivity, the ζ potential is always deduced from the experimental values of C_S, of ρ_f, and of the ratio F/F_0 using (33) and a numerical value of η/ε = 14 (at 25°C), with C_S expressed in mV/0.1 MPa, ρ_f in Ω m, and ζ in mV.

3. Experimental Setup

3.1. Sample Assembly and Fluid Circulation

The experimental setup is depicted in Figure 2. The crushed sample was placed in a glass cylinder having a diameter of 4 cm. The cylinder was closed at both ends by insulating polymer plugs with O-rings. The interstitial electrolyte flowed through 6 mm diameter channels drilled in the polymer plugs. Stainless steel electrodes, located at both ends of the sample, were used for the electrical measurements. The electrodes each contain three holes with a diameter of 6 mm, and radial groves are machined on the face in contact with the sample in order to spread the fluid flow uniformly into and out of the sample. The length of the porous sample varied between 7 and 8 cm. Stainless steel grids (with spacing varying from 100 to 315 μm) are inserted between the polymer plugs and the electrodes to avoid sample grains leaving the assembly. For grain sizes >300 μm the standard electrodes were not used, and the grids were used as electrodes instead. For some measurements, additional stainless steel grid electrodes were also inserted at various depths in the sample.

The samples were crushed rocks with a known grain size range, defined by two sieve grid sizes. Each sample was then characterized by the average between the defining sieving grids. The permeability range varied from 50 mdarcy to >100 darcies. Most measurements were performed with crushed Fontainebleau sandstone, which is composed of >99% quartz.

The electrolyte was circulated from a large container to the

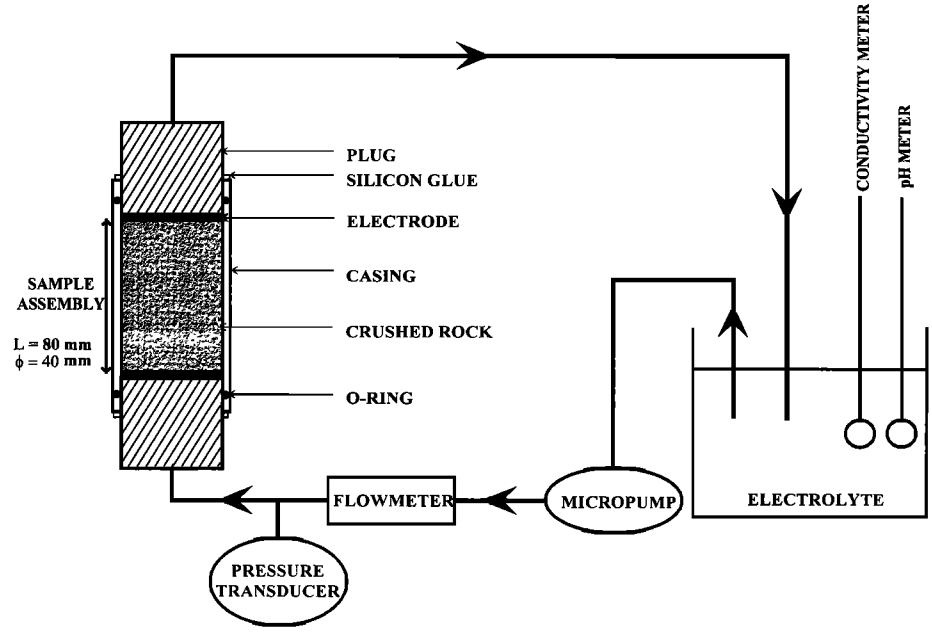

Figure 2. The experimental setup used for the measurement of streaming potentials with crushed rock samples.

sample using a micropump with controlled flow rate. The maximum flow rate used for measurements was 500 mL/min. The pressure head at the pump output was measured using a high-precision pressure sensor (RDP Electronics) with an uncertainty of ±0.35 kPa. The outlet was always at atmospheric pressure. The head loss corrections to obtain the pressure difference across the sample are significant: they amount to ~5–6 kPa for the maximum flow rate. These head loss corrections were calculated and have been regularly checked experimentally by making pressure measurements without any sample in the cell. The permeability of the sample was determined from the measurement of the flow rate, using a precision Mettler balance, or with the flowmeter for large flow rate. For small permeabilities the flowmeter was not accurate enough and was not included in the setup.

This setup has been chosen in order to maximize the pressure gradient across the sample and consequently the related electrical signal. However, the flow of electrolyte through the sample can change the configuration of the sample, especially for small grain sizes (<60 μm) for which grains are dragged to the electrode grids, inducing a reduction of permeability. In order to avoid such problems the permeability of several samples of a given grain size was measured for a given constant flow rate. The permeability distribution for a given grain size was then derived. During all subsequent experiments, if the permeability of a given sample diverged significantly from an allowed range (±3 standard deviations or so), the experiment was stopped.

The flow rate in all cases has to be maintained at a reasonable value, even for large grain sizes. For large grain sizes, large flow rates introduce nonlaminar flow and a localization of the flow pattern in preferred paths. The permeability from such patterns is usually unstable and nonreproducible. These problems can be avoided by requiring a stable permeability, namely, a constant pressure for a given flow rate set by the pump.

3.2. Electrical Measurements

Stainless steel electrodes were used for the electrical measurements, as it was found that the polarization potentials could be corrected for. For this purpose, the electrical potentials were measured as a function of time with a sampling time of 1 s or less, depending on the experiment. The observed drift of the electrode was between 0.1 and 1 mV/min for the worst cases in which corrosion of the electrodes occurred. The alloy of the electrode (stainless steel type SS316L) was chosen because it is used with success under high-salinity conditions in marine measurements with minimal corrosion. When necessary, the electrode drift was corrected for by interpolating a straight line during the application of the pressure gradient and by subtracting the average interpolated value from the average measured potential difference. This correction introduces an uncertainty of 20–40% for the smallest measured streaming potential coefficient (4 mV/0.1 MPa). For most measurements presented in this paper, however, the resulting experimental uncertainty is <1%.

The electric potential was measured by a high-precision HP34401A voltmeter, with an input impedance of 1 GΩ. This high input impedance is necessary for measuring samples at the higher electrolyte resistivities [*Morgan et al.*, 1989].

For practical reasons, especially for high flow rates, it is considerably easier to use a closed circulation loop because the amount of electrolyte to be prepared is much smaller and a large number of experiments can be performed. Also, recirculation of the fluid helps maintain a chemical equilibrium between the sample and the electrolyte and reduces diffusion electric potentials to zero [*Bard and Faulkner*, 1980]. Since the electrolyte is circulating in a closed loop, there is, in principle, a leakage resistance in parallel with the sample between the two electrodes used for the electric potential measurement. All elements of the circuit are made of insulating polymers. The length and cross section of the tubes were chosen such that the

leakage resistance is <1% of the sample resistance, even for the largest formation factors used during the experiment ($F \approx 5$). This fact was also checked experimentally by having the exit tube in another reservoir.

For streaming potential measurements it is also necessary to check the size of the so-called motoelectrical effect [*Ahmad*, 1964]. This effect is the production of spurious potentials produced by the electrodes when the electrolyte is circulated. The physical origin of this effect is not well understood, but it is most likely associated with the electrical double layer at the metal-electrolyte interface. This effect is known to be large (~95 mV) for platinum [*Ogilvy et al.*, 1969]. The effect has been measured in our setup without a rock sample as a function of pressure and electrolyte resistivity. It amounts to ~2 mV/0.1 MPa but is not linear with pressure or electrolyte resistivity. Given the small size of this effect, as the electrolyte resistivity was always >10 Ω m and the ζ potential larger than a few mV, it was neglected for the data interpretation.

The resistivity of the sample was measured using a HP34263A ohm meter at the fixed frequency of 1 kHz (real part of the response), with two or four electrodes. For the four-electrode measurements, two additional grids were inserted in the sample. The measuring setup (electrodes plus wires) was checked with calibrated resistors. At the highest values of the resistance (>20 MΩ, corresponding to values of the electrolyte resistivity >8000 Ω m) the calibration was found to give incorrect results with some of the cables used. Cables have to be as short as possible to maintain accuracy for the higher values of electrolyte resistivities.

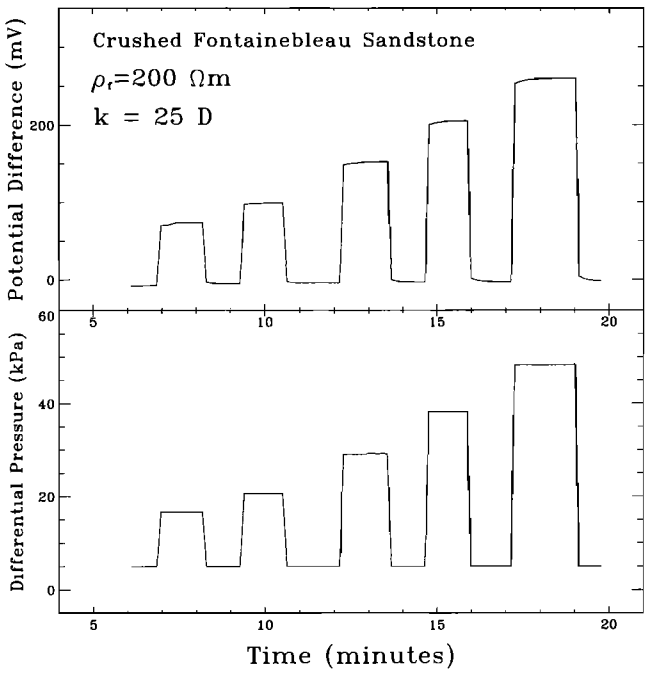

Figure 3. A typical streaming potential experiment with crushed Fontainebleau sandstone. The electric potential difference between the two electrodes is shown as a function of time, together with the applied pressure difference across the sample. The electric potential reference is taken at the high-pressure end [*Morgan et al.*, 1989].

3.3. Chemical Measurements

The electrolyte conductivity was measured by a CDM92 precision conductimetry cell that was regularly calibrated against reference solutions. The conductivity was measured in the reservoir after preparation of the electrolyte and was measured during the flow experiments at the outlet, with the sampling time mentioned before.

The pH of the electrolyte was measured using a METROHM electrode. For high resistivities the pH measurement using the standard pH electrode saturated with KCl is not accurate enough, and the pH of such solutions was checked using dedicated electrodes and precise titrometry.

The electrolytes were prepared using degassed deionized water with a resistivity of 40,000 Ω m, which was considered as pure water. At room temperature, under normal working conditions, the pH of the solution is constrained by the electrolytes used and the dissolution of atmospheric CO_2. Pure water in equilibrium with the atmosphere reaches after 1 day a resistivity varying between 10,000 and 12,000 Ω m and a pH between 5.4 and 5.8, in agreement with the theoretical values of 12,700 Ω m and pH = $3.9 - 1/2 \log_{10} p_{CO_2}$, respectively, where p_{CO_2} is the partial pressure of CO_2 in atmosphere [*Sigg et al.*, 1992]. The partial pressure of CO_2 under normal conditions is 3×10^{-4} atm.

The laboratory is thermally isolated, and its temperature is maintained constant within 0.5 to 1°C of 22°C using feedback air conditioning. All experiments were thus performed at the same temperature.

3.4. Experimental Protocol and Checks

After installation of the crushed sample in the assembly and before starting the measurements, the sample was cleaned by circulating successive reservoirs of pure water for several hours, until the final water conductivity reached a stable value. The permeability was measured and checked to be within the allowed range corresponding to the sample's grain size. The electrolyte was then circulated through the sample until the conductivity was stable, ensuring that a chemical equilibrium had been reached. This procedure ensures that the measurements are reproducible within 5%, even if the sample is left in contact with the electrolyte for some days.

The potential measurement during a typical streaming potential experiment is displayed in Figure 3. Circulation of the electrolyte produces clear electrical signals. The stability of the electrodes allows a streaming potential as low as 0.5 mV to be measured reliably. Because the signal is proportional to the product $\zeta \rho_f$ (equation (37)), a precision >5% on ζ requires that the value of the electrolyte resistivity usually must be >10 Ω m.

The streaming potential coefficient is displayed as a function of the pressure gradient in Figure 4, showing that a deviation from linearity is observed only for pressures >50 kPa, corresponding to flow rates >90 mL/min for the permeability of this sample. Flow rates <20 mL/min were used for the measurements of streaming potentials reported in this paper.

It is important to check that the electrolyte resistivity has reached a stable value and that it is the same at the input point and the exit point of the sample. Concentration gradients in the electrolyte might result in diffusion or membrane potentials. These potentials can be larger than a few mV for salts like NaCl that have different cation and anion diffusion coefficients [*Bard and Faulkner*, 1980].

In order to check the homogeneity of the electrical signal in the crushed sample, some experiments were performed with additional grid electrodes interspersed at several positions

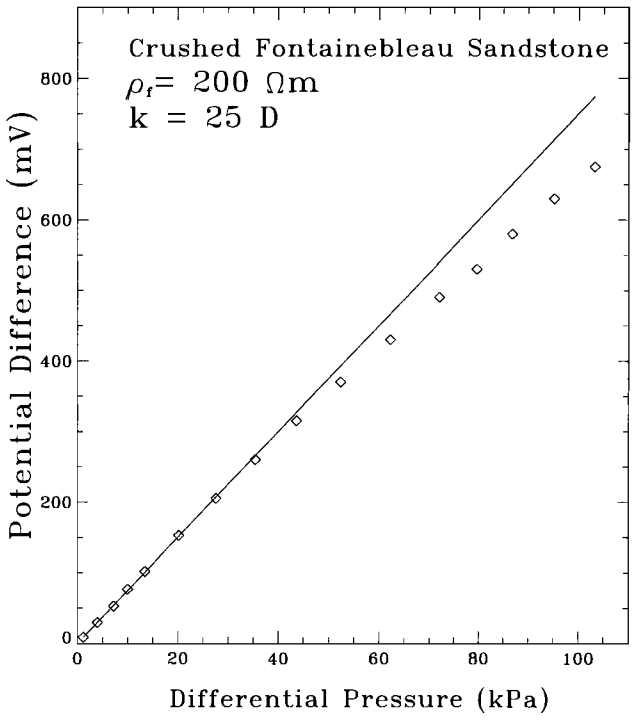

Figure 4. The streaming potential as a function of the applied pressure gradient. The maximum pressure gradient used for the measurements of streaming potentials at this permeability was 30 kPa.

along the sample. The potentials measured with the additional electrodes demonstrated that the electric field is homogeneous inside the sample to better than 3% and that no edge effect affect the measurement with the end electrodes.

In order to compute the ζ potential using (33) the correction factor F/F_0 was obtained from the data using resistance measurements:

$$\frac{F}{F_0} = \frac{\rho_0}{\rho_f}\frac{R(\rho_f)}{R(\rho_0)}, \tag{36}$$

where ρ_0 is an electrolyte resistivity where the contribution of surface conductivity is negligible.

For Fontainebleau sandstone the surface conductivity varies from 0.01 to 0.08 mS/m, as illustrated in Figure 5, in agreement with previous studies [*Ruffet et al.*, 1991]. The contribution of surface conductivity is therefore always <1% for electrolyte resistivities <30 Ω m, and the ratio F/F_0 can be measured using ρ_0 = 10 or 30 Ω m in (36).

4. Results and Discussion

4.1. The ζ Potential for Fontainebleau Sandstone

The ζ potential values, inferred from the streaming potentials measured in these experiments with crushed Fontainebleau sandstone, were significantly smaller (in absolute value) than the values reported for quartz [*Ishido and Mizutani*, 1981], Westerly granite [*Morgan et al.*, 1989], or some of the values found previously for Fontainebleau sandstone [*Jouniaux and Pozzi*, 1995b]. For example, for a KCl solution of 400 Ω m resistivity at pH = 5.7, we find $\zeta = -40 \pm 5$ mV, where the error (1 standard deviation) is dominated by sample to sample variations, compared with some values ranging to −100 mV or larger from the aforementioned papers. For the sample used for this measurement, at ρ_f = 400 Ω m, the surface conductivity correction (F/F_0 of (36)) is negligible (<1%).

In order to check whether this discrepancy was due to the fact that the Fontainebleau sandstone may contain a small fraction of carbonates, one experiment was performed after the crushed sample was cleaned with concentrated hydrochloric acid for 3 days and then washed with pure water for >24 hours. The ζ potential obtained from the streaming potentials measured after this procedure was $\zeta = -51$ mV, compared with a value −47 mV before, indicating that our measurements are not significantly affected by the fact that the samples were not cleaned with acid. The measurements presented for Fontainebleau sandstone should therefore reflect processes at the electrolyte-quartz interface.

4.2. Effect of Electrolyte Resistivity

Results of the measurements of the ζ potential as a function of electrolyte resistivity for KCl are shown in Figure 6. The data show an increase with electrolyte resistivity of ~20 mV per decade, in agreement with the compilation of *Pride and Morgan* [1991]. Between 40 and 1000 Ω m, the ζ potential for KCl for crushed Fontainebleau sandstone (CFS) at pH = 5.7 was measured to be

$$\zeta_{CFS}(\text{pH} = 5.7) = -26 \text{ mV} \left(\frac{\rho_f}{100}\right)^{0.23 \pm 0.014}, \tag{37}$$

for electrolyte resistivity expressed in Ω m.

The highest resistivity was obtained using pure water, without added KCl. The data were acquired by progressively adding salt to the solution, and each measurement is made after

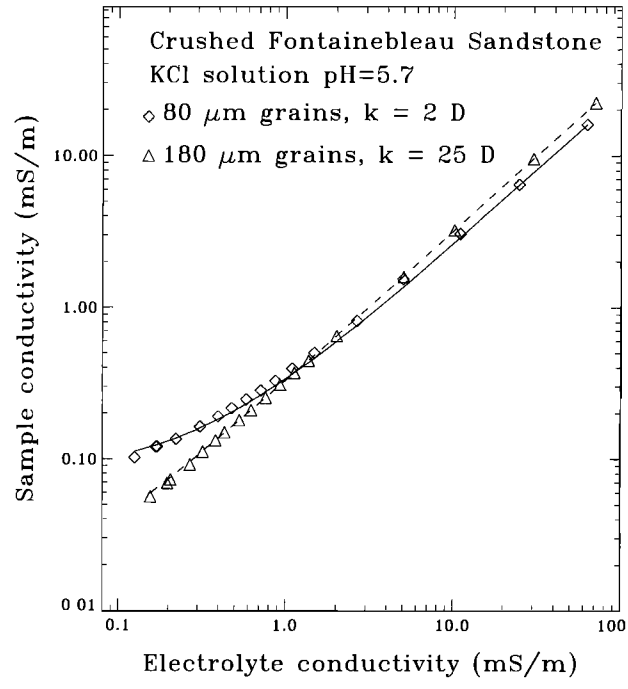

Figure 5. The sample conductivity as a function of the electrolyte conductivity for two samples of crushed Fontainebleau sandstone with different grain sizes. The experimental errors are of the order of the size of symbols. The solid (dashed) line corresponds to a surface conductivity of 0.08 mS/m (0.01 mS/m).

waiting 20–30 min to ensure chemical equilibrium between the solution and the sample. Several measurements were made at each resistivity, and it was regularly checked that the sample permeability was not changing during the experiment.

For electrolyte resistivities >1000 Ω m the ζ potential does not follow the scaling of (37). For these values of resistivity the surface conductance makes a significant contribution to sample conductivity, although the measurements were performed for a grain size for which the surface conductivity is smallest (see Figure 5). The correction factor F/F_0 of (36) indeed varies from 0.95 at 10^3 Ω m to 0.7 at 10^4 Ω m.

The data are compared with the predictions of the three-layer model in Figure 6, with the parameters indicated. The values used for the capacitances C_1 = 100 μF/cm^2 and C_2 = 20 μF/cm^2 are taken from *Davis et al.* [1978]. The value of the equilibrium constant pK_- is the value recommended by *Revil and Glover* [1997] and close to the value pK_- = 7.2 used by *Davis et al.* [1978]. When pH is around 5.7, as in Figure 6, the calculated result is insensitive to the value of the pzc. The value pK_K = 4 is rather high compared with the value pK_K = 6.7 proposed by *Davis et al.* [1978]. The value of pK_{Cl} was not measured by *Davis et al.* [1978]; we used pK_{Cl} = −9 to match the experimental data. This value can be compared with the value pK_{Cl} = −4.5 found by *Davis et al.* [1978] for a TiO_2-KNO_3 interface. With these values of the parameter the three-layer model does reproduce the behavior of the experimental data up to an electrolyte resistivity of 2000 Ω m.

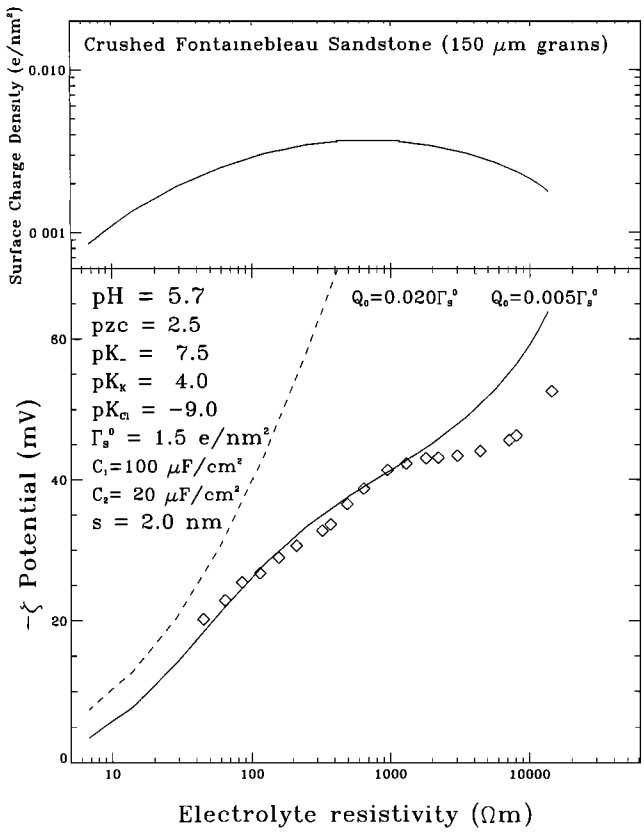

Figure 6. The ζ potential, inferred from streaming potential measurements using crushed Fontainebleau sandstone, as a function of electrolyte resistivity for KCl solutions with pH = 5.7. The measurement experimental errors are of the size of the symbols. The solid line corresponds to the prediction of the three-layer model [*Davis et al.*, 1978] using the parameters indicated. The dotted and dashed lines correspond to simple calculations of the ζ potential assuming a constant surface charge density $Q_S = -Q_0$ at the Stern plane, with $Q_0 = 0.005\Gamma_S^0$ and $0.020\Gamma_S^0$.

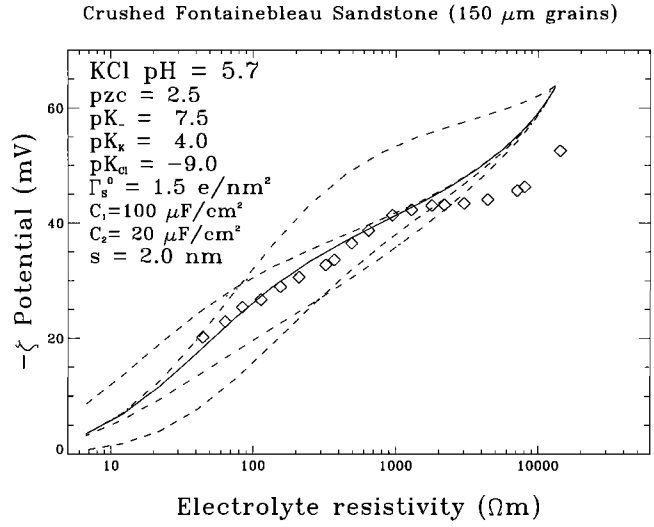

Figure 7. The ζ potential, inferred from streaming potential measurements using crushed Fontainebleau sandstone, as a function of electrolyte resistivity for KCl solutions with pH = 5.7. The measurement experimental errors are of the size of the symbols. The lines correspond to the predictions of the three-layer model [*Davis et al.*, 1978]. The solid line correspond to the default parameters indicated. The dotted line refers to the related Stern plane potential. The dashed lines correspond to pK_{K^+} increased or decreased by 1. When K_{K^+} is increased, the absolute value of the ζ potential is decreased. The dash-dotted lines correspond to pK_{Cl} increased or decreased by 1. When K_{Cl} is increased, the absolute value of the ζ potential is increased.

The predictions of simple models having fixed surface charge densities of $Q_0 = 0.005\Gamma_S^0$ and $0.020\Gamma_S^0$, independent of the Stern plane potential, are also shown in Figure 6 for comparison. These curves are obtained by inserting the indicated constant value in (30). The slopes predicted by the models with fixed surface charges are 3–4 times larger than the data. The surface charge density predicted by the three-layer model varies from $Q_0 = 0.004\Gamma_S^0$ for ρ_f = 700 Ω m to $Q_0 = 0.001\Gamma_S^0$ for ρ_f = 10 Ω m. Note that 100 Ω m of KCl corresponds to ~1 mmol/L. The data therefore support the physical relationship between the surface charge density and the electrolyte concentration predicted by the three-layer model of the EDL, as recognized by *Davis et al.* [1978, and references therein].

The effect of changing some parameters of the three-layer model is shown in Figures 7 and 8. Increasing the value of the K_K constant decreases the absolute value of the ζ potential at the lower values of the electrolyte resistivity. This is due to the fact that the contribution of the K_K constant to the surface charge density Q_2 is proportional to the salt concentration (equation (11)). More K^+ ions are adsorbed for higher K_K, thus compensating a greater fractions of the Si − O^- sites. Increasing the value of the K_{Cl} constant has the opposite effect: the absolute value of the ζ potential is increased if the value of K_{Cl} is decreased, and the effect is larger at resistivities ~1000 Ω m.

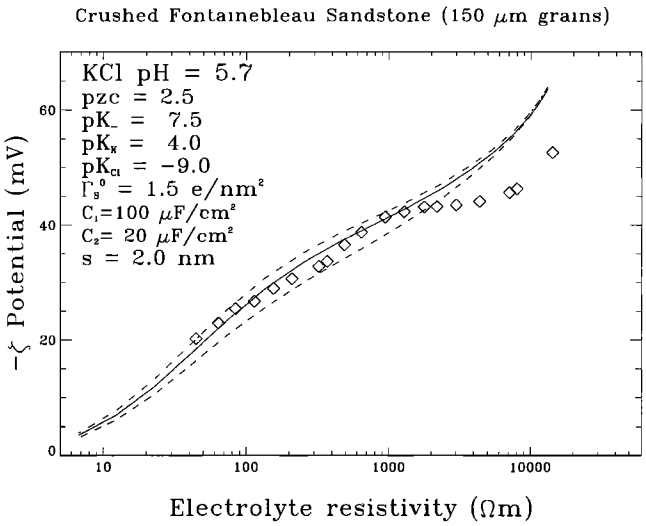

Figure 8. The ζ potential, inferred from streaming potential measurements using crushed Fontainebleau sandstone, as a function of electrolyte resistivity for KCl solutions with pH = 5.7. The measurement experimental errors are of the size of the symbols. The lines correspond to the predictions of the three-layer model [*Davis et al.*, 1978]. The solid line corresponds to the default parameters indicated. The dashed line corresponds to a C_1 capacitance twice as large. The dash-dotted line corresponds to a C_2 capacitance twice as large.

The overall scale of the ζ potential is defined approximately by the product $K_-\Gamma_S^0$ (equation (9)), and the values of K and Γ_S^0 are hard to determine independently from the data. In a first approximation, using a higher value for the total surface charge site density is equivalent to increasing pK_-.

The sensitivity of the theoretical prediction to the value of the s parameter is also shown in Figure 7, where the calculated Stern plane potential (dotted line) is compared with the ζ potential (solid line). Using a nonzero s parameter introduces a small reduction of the absolute value of the ζ potential for small values of the electrolyte resistivity (20% at ρ_f = 100 Ω m, 50% at ρ_f = 10 Ω m). This is due to the decrease of the Debye screening length when the ion concentration is increased (equation (29)). The Debye length for a solution of KCl is ~10 nm/$\sqrt{c}$, where c is the KCl concentration in mmol/L. The effects of introducing a nonzero s parameter and of changing the values of the equilibrium constants are not exactly equivalent as a function of resistivity. However, the data would also fit a model with s = 0, a smaller value of the K_{Cl} parameter, and a larger value of the K_- equilibrium constant.

In Figure 8 the sensitivity of the prediction of the three-layer EDL model to the values of the capacitances C_1 and C_2 is illustrated. The ζ potential at pH = 5.7 has little sensitivity to the values of the capacitances.

For values of resistivity >5000 Ω m, however, the data show a smaller rate of increase with electrolyte resistivity, and the three-layer model overestimates the data in this region. This change of slope at high resistivity was observed for almost all electrolytes. For such high resistivities the concentration of KCl is actually smaller than the concentrations of H^+ and HCO_3^-, and the properties of the EDL are actually controlled by the H^+ and HCO_3^- ions. This fact is taken into account in the theoretical curves shown in Figures 6 and 7 and is thus not sufficient to explain the data, indicating that the chemical phenomena must be more complex in this region. The validity of (33) in this region is discussed by *Lorne et al.* [this issue].

In Figure 9 the experimental results are compared with the prediction of the simplified single-layer model [*Revil and Glover*, 1997] presented earlier in section 2.2 (see equation (19)). The values of the parameters indicated on Figure 9 are close to the values recommended by *Revil and Glover* [1997]. This simplified model explains the dependence of the ζ potential as a function of the electrolyte resistivity about as well as the three-layer model. In this model the surface charge density for pH < 7 can be approximated by (equation (19))

$$Q_0(\varphi_0) = \Gamma_S^0 \frac{K_-}{c_{H^+}^0} \exp\left(2\frac{\varphi_0}{v_0}\right), \tag{38}$$

as the K_{Cl} and K_K terms can be neglected. In the case of a 1:1 electrolyte the Poisson-Boltzmann equation can be integrated analytically, and (30) gives [*Bard and Faulkner*, 1980]

$$Q_0(\varphi_0) = -0.022\sqrt{c_{KCl}}\sinh\left(\frac{\varphi_0}{v_0}\right) e/\text{nm}^2. \tag{39}$$

When the concentration of KCl increases, the absolute value of the Stern plane potential decreases to maintain the equality between (38) and (39). The physical origin of the resistivity dependence of the ζ potential is then the fact that the concentration of H^+ ions on the mineral surface is increased for higher absolute values of the Stern plane potential. When more ions are present in the solution, the Stern plane electric charge is screened more efficiently and a lower electric potential develops (see equation (39)). However, this reduction is damped by the fact that the enhancement of the H^+ concentration on the mineral surface is less efficient, and hence more $Si-O^-$ species are produced by reaction (1) to maintain the equilibrium (equation (38)).

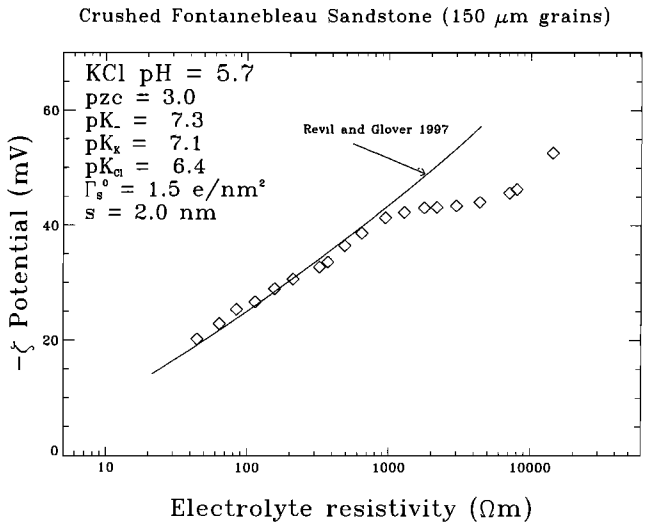

Figure 9. The ζ potential, inferred from streaming potential measurements using crushed Fontainebleau sandstone, as a function of electrolyte resistivity for KCl solutions with pH = 5.7. The measurement experimental errors are of the size of the symbols. The lines correspond to the predictions of a simplified one-layer model [*Revil and Glover*, 1997]. The solid line corresponds to the default parameters indicated. The dotted line refers to the related Stern plane potential.

4.3. Effect of pH

The ζ potential is shown as a function of pH for NaCl in Figure 10 and for KCl in Figure 11. For the data in Figure 10, pH was adjusted by adding HCl (pH < 5.7) or NaOH (pH > 5.7) and the conductivity of the solution was adjusted by adding NaCl. In Figure 10, most measurements correspond to an electrolyte resistivity of 100 Ω m; however, for pH < 3.3 and pH > 10.2 it was not possible to obtain the desired pH and to maintain a resistivity of 100 Ω m. In Figure 11, pH was adjusted using KOH instead of NaOH, and all measurements with KCl were performed with a solution resistivity of 25.5 Ω m.

In Figure 10 the change of sign of the ζ potential when crossing the pzc is clearly observed. The value of the pzc is measured to be 2.5 ± 0.1. The shape of the pH dependence is in good agreement with the measurements of *Ishido and Mizutani* [1981], *Somasundaran and Kulkarni* [1973], or *Massenet and Pham* [1985b]. The absolute value of the ζ potential reported by *Ishido and Mizutani* [1981], however, is 2–3 times larger. A pzc close to 4.5 was measured by *Massenet and Pham* [1985b] for volcanic ashes from Mount Etna. The value of the pzc depends on the minerals present in the sample [*Ishido and Mizutani*, 1981]. *Somasundaran and Kulkarni* [1973] reported a steeper variation with pH than observed in this experiment or by other workers.

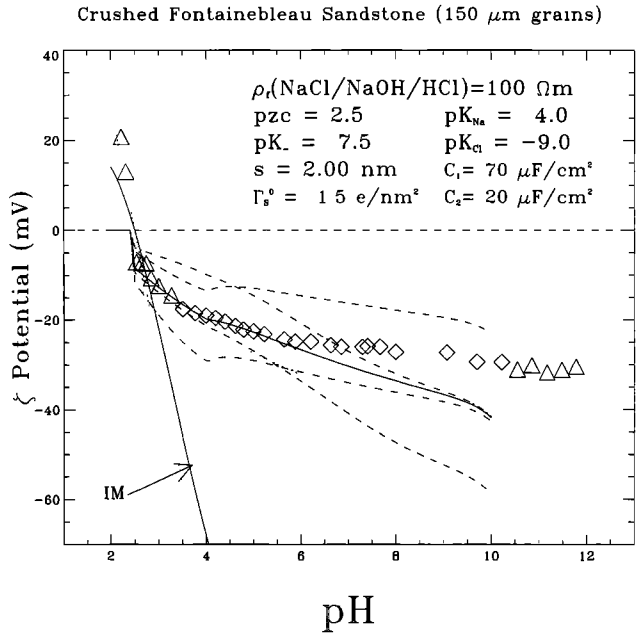

Figure 10. The ζ potential, inferred from streaming potential measurements using crushed Fontainebleau sandstone, as a function of pH for NaCl/HCl/NaOH solutions. Diamonds correspond to measurements with an electrolyte resistivity of 100 Ω m. Triangles correspond to measurements for which the electrolyte resistivity is controlled by the pH and can not be maintained at 100 Ω m. The measurement experimental errors are of the size of the symbols. The lines correspond to the predictions of the three-layer model [*Davis et al.*, 1978]. The solid line corresponds to the default parameters indicated. The dotted line refers to the related Stern plane potential. The dashed lines correspond to pK_{Na} increased or decreased by 1. When K_{Na} is increased, the absolute value of the ζ potential is decreased. The dash-dotted lines correspond to pK_{Cl} increased or decreased by 1. When K_{Cl} is increased, the absolute value of the ζ potential is increased. The prediction from *Ishido and Mizutani* [1981] is also shown for comparison (IM).

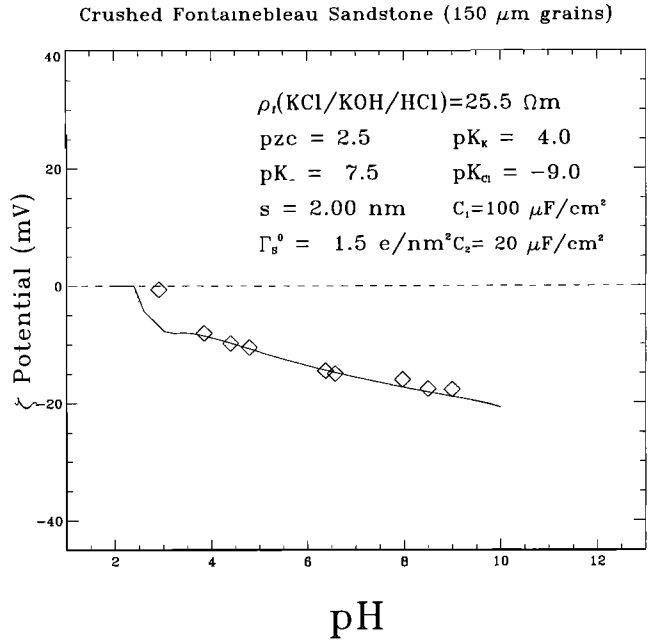

Figure 11. The ζ potential, inferred from streaming potential measurements using crushed Fontainebleau sandstone, as a function of pH for KCl/HCl/KOH solutions with a resistivity of 25.5 Ω m. The measurement experimental errors are of the size of the symbols. The lines correspond to the predictions of the three-layer model [*Davis et al.*, 1978]. The solid line corresponds to the default parameters indicated. The dotted line refers to the related Stern plane potential.

For pH from 5.7 to 8, which is the domain for most applications with natural groundwater, the observed variations are approximately linear and can be represented by

$$\zeta_{CFS}^{NaCl}(\rho_f = 100\ \Omega\ m, pH) = \zeta_{CFS}^{NaCl}(\rho_f = 100\ \Omega\ m, pH = 5.7) \cdot [1 + (0.068 \pm 0.004)(pH - 5.7)] \quad (40a)$$

$$\zeta_{CFS}^{KCl}(\rho_f = 25\ \Omega\ m, pH) = \zeta_{CFS}^{KCl}(\rho_f = 25\ \Omega\ m, pH = 5.7)[1 + (0.14 \pm 0.02)(pH - 5.7)] \quad (40b)$$

The measurements are compared with the three-layer EDL model in Figures 10, 11, and 12. The three-layer model, with the values of the parameters used in the previous discussion, accommodates well the experimental data. For NaCl, a value of $C_1 = 70\ \mu F/cm^2$ was used. In Figure 10 the model calculation is sensitive to the values of the parameters, in particular for pH close to pzc. If the value of the K_{Na} constant is increased, the scale of the ζ potential is reduced, especially for increasing pH, and the slope for pH > 6 is also reduced. The model prediction is most sensitive to the value of the K_{Cl} constant for pH between pzc and 5. The model prediction may deviate significantly from the experimental data if large changes in the parameters are imposed, for example, by using constraints from other chemical data.

The Stern plane potential is also displayed in Figure 10, for the indicated values of the parameters, to illustrate the effect of a nonzero s parameter. As shown previously by *Ishido and Mizutani* [1981], the pH variation of the ζ potential is sensitive

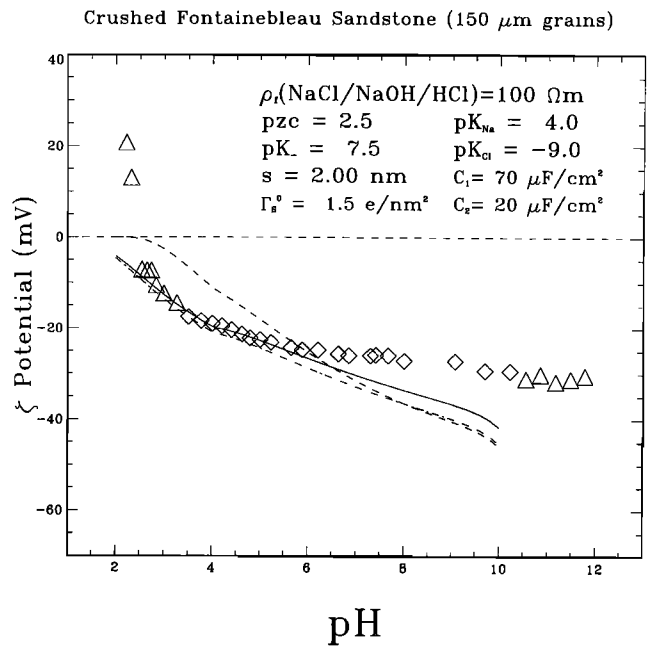

Figure 12. The ζ potential, inferred from streaming potential measurements using crushed Fontainebleau sandstone, as a function of pH for NaCl/HCl/NaOH solutions. Diamonds correspond to measurements with an electrolyte resistivity of 100 Ω m. Triangles correspond to measurements for which the electrolyte resistivity is controlled by the pH and cannot be maintained at 100 Ω m. The measurement experimental errors are of the size of the symbols. The lines correspond to the predictions of the three-layer model [*Davis et al.*, 1978]. The solid line corresponds to the default parameters indicated. The dashed line corresponds to a C_1 capacitance twice larger. The dash-dotted line corresponds to a C_2 capacitance twice larger.

to the value of the s parameter, and the pH dependence can be used to derive its value. Compared with the resistivity dependence, the slope of the pH dependence is more decoupled from the values of the equilibrium constants. The data in Figure 10 would be better described by a three-layer model with s = 4 nm; however, this would cause the predicted pH dependence to deviate from the KCl data in Figure 11. Although using s = 2 nm provides a good agreement with the data, the data are not incompatible with s = 0.

The *Ishido and Mizutani* [1981] model is also shown in Figure 10. This model predicts the correct overall shape of the pH dependence, but the scale of the potential is too high for pH > 3.5. The value of the resistivity exponent of (37) predicted by this model is 0.14 for pH = 5.7, in contrast with the observed value of 0.23 ± 0.014.

In Figure 12 the effect of changing the values of C_1 and C_2 is illustrated. Increasing the value of the C_2 parameter by a factor of 2 has little effect on the ζ potential. However, the dash line, calculated with a C_1 parameter increased by a factor of 2, shows a reduction of the absolute value of the ζ potential by a factor 2 or more for pH < 5. The fact that the ISCP and OSCP do not coincide is then a crucial aspect of the EDL. This fact is also illustrated in Figure 13, where the measurements are compared with the predictions of the one-layer model [*Revil and Glover*, 1997]. Their model does not accommodate the measured pH variations, even if large excursions of its parameters are allowed (dashed line). A three-layer model appears necessary to describe the physical processes of the EDL [*Davis et al.*, 1978; S. Pride, private communication, 1997].

The slope of the ζ potential with electrolyte resistivity in the three-layer model depends on the pH, as depicted in Figure 14. For pH = 7.5 the dependence of the ζ potential on the electrolyte resistivity is increased by almost a factor of 2 compared with pH = 5.7. The ρ_f exponent defined in (37) predicted by the three-layer model is shown in Figure 15 as a function of pH. One should therefore be careful when applying the experimentally measured value 0.23 to values of pH significantly different from 5.7. In addition, the three-layer model overestimates the slope at pH = 5.7, a fact that can be seen in Figure 6 for values of electrolyte resistivity <100 Ω m.

Similarly, the predicted slope of the ζ potential as a function of pH between 5.7 and 8, shown in Figure 16, is sensitive to the value of the electrolyte resistivity. The three-layer EDL model tends to overestimate the pH dependence compared with the observations. The predictions of the three-layer model should therefore be taken with caution, and one should rather rely on experimental measurements when they are available.

4.4. Effect of the Valence and the Size of the Ions

The effect of changing the valence of one of the ions is illustrated in Figure 17, where measurements with KCl, K_2SO_4, $CaCl_2$, and $CaSO_4$ are compared as a function of the electro-

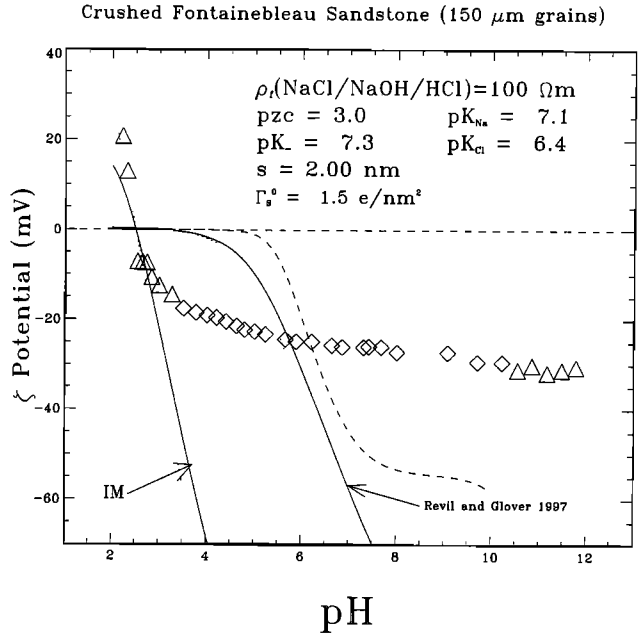

Figure 13. The ζ potential, inferred from streaming potential measurements using crushed Fontainebleau sandstone, as a function of pH for NaCl/HCl/NaOH solutions. Diamonds correspond to measurements with an electrolyte resistivity of 100 Ω m. Triangles correspond to measurements for which the electrolyte resistivity is controlled by the pH and cannot be maintained at 100 Ω m. The measurement experimental errors are of the size of the symbols. The lines correspond to the predictions of a simplified one-layer model [*Revil and Glover*, 1997]. The solid line corresponds to the default parameters indicated. The dotted line refers to the related Stern plane potential. The dashed line correspond to the parameters of the three-layer model indicated in Figure 11. The prediction from *Ishido and Mizutani* [1981] is also shown for comparison (IM).

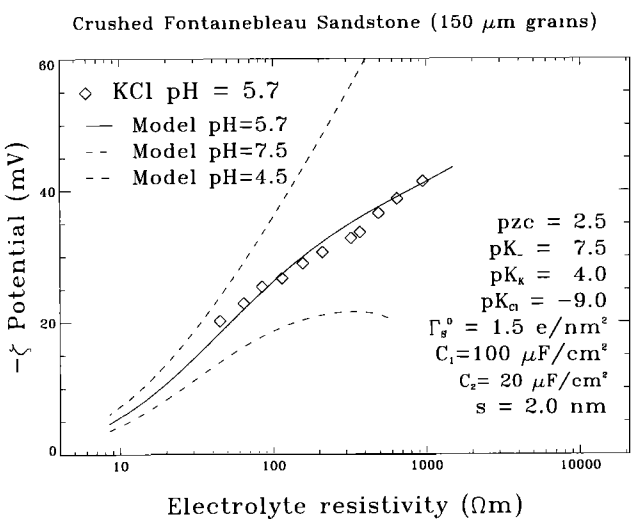

Figure 14. The ζ potential, inferred from streaming potential measurements using crushed Fontainebleau sandstone, as a function of electrolyte resistivity for KCl solutions with pH = 5.7. The measurement experimental errors are of the size of the symbols. The solid line corresponds to the prediction of the three-layer model [*Davis et al.*, 1978] using the parameters indicated. The dashed and dash-dotted lines correspond to the predictions for pH = 7.5 and pH = 4.5, respectively.

lyte resistivity. Experiments using KCl were repeated, in between these other salts, to check the reproducibility of the streaming potential, and the pH was measured for each salt and for each value of streaming potential coefficient. The highest resistivity (12,000 Ω m) is achieved using pure water, and the coincidence of the data illustrates the excellent reproducibility of the streaming potential measurements.

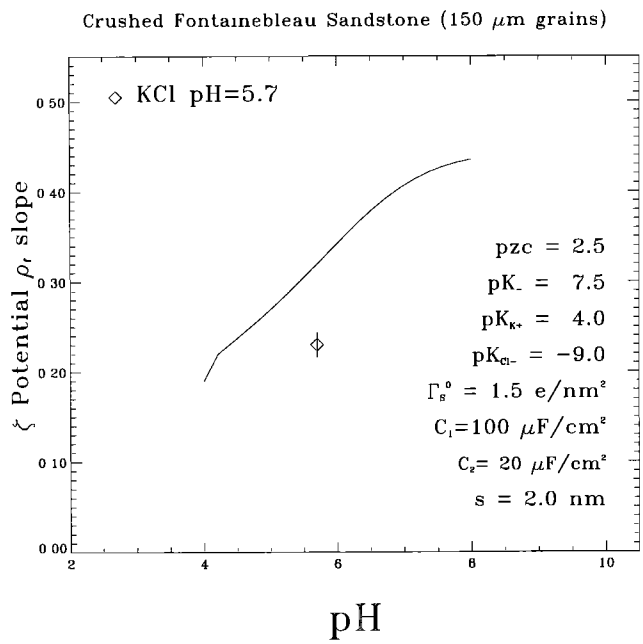

Figure 15. The exponent parameter α as a function of pH, where α is defined as $\zeta = (\rho_f)^{\alpha}$. The exponent is calculated from 50 to 300 Ω m. The solid line corresponds to the prediction of the three-layer model [*Davis et al.*, 1978] using the parameters indicated.

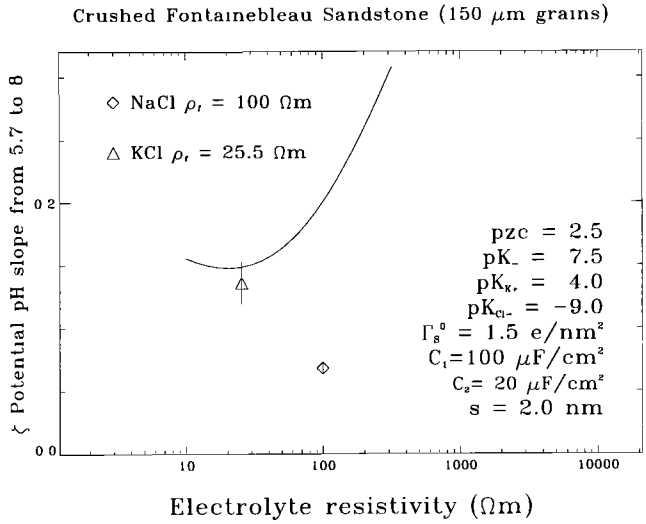

Figure 16. The relative variation of the absolute value of the ζ potential from pH = 5.5 to pH = 8, as a function of the electrolyte resistivity. The solid line corresponds to the prediction of the three-layer model [*Davis et al.*, 1978] using the parameters indicated.

When even small quantities of salt are added to the solution, a greater reduction of the ζ potential is observed for divalent cations than for monovalent ions, as mentioned by *Morgan et al.* [1989] and *Davis et al.* [1978]. A divalent cation will indeed shield the negative charge of the EDL more efficiently.

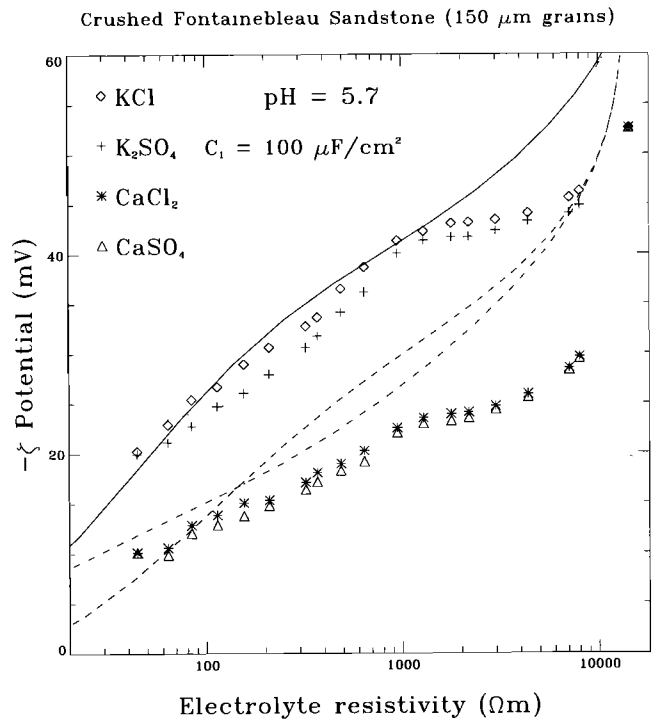

Figure 17. The ζ potential, inferred from streaming potential measurements using crushed Fontainebleau sandstone, as a function of electrolyte resistivity for several salt solutions with pH = 5.7, changing the valence of the ions. The lines correspond to the predictions of the three-layer model [*Davis et al.*, 1978] with the parameters indicated in Table 1, from top to bottom KCl, K_2SO_4, $CaCl_2$, and $CaSO_4$.

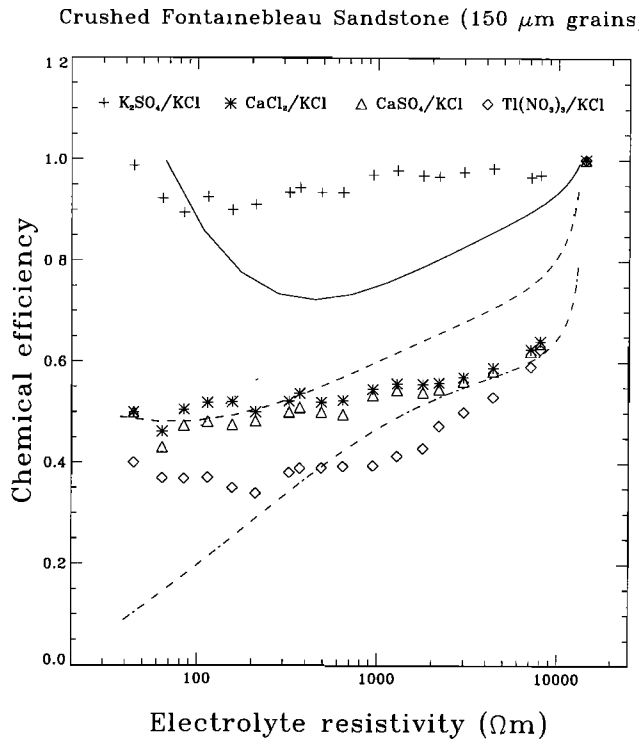

Figure 18. The streaming potential chemical efficiency as a function of electrolyte resistivity for several salt solutions with pH = 5.7. The measurement experimental errors are of the size of the symbols. The lines correspond to the predictions of the three-layer model [*Davis et al.*, 1978] with the parameters indicated in Table 1, from top to bottom K_2SO_4, $CaCl_2$, $CaSO_4$, and $Tl(NO_3)_3$.

Let us define the ratio of the ζ potential for a given solution to the ζ potential for KCl at the same resistivity as the streaming potential chemical efficiency, noted E_S. It can be seen in Figure 18 that the experimental values of the chemical efficiency are almost independent of the electrolyte resistivity from 40 to 2000 Ω m, in contrast with what can be inferred from earlier results [*Morgan et al.*, 1989]. The experimental values, listed in Table 1, cluster around 1 for monovalent ions and 0.5 for divalent cations.

The accommodation of divalent cations in the three-layer theory is not straightforward. The curves shown in Figure 17 have been calculated assuming the following adsorption reactions [*Davis et al.*, 1978]:

$$\mathrm{Si-OH} + \mathrm{M}^{n+} \overset{K_M}{\longleftrightarrow} \mathrm{Si-O-M}^{+(n-1)} + \mathrm{H}^+, \quad (41)$$

$$\mathrm{Si-OH} + \mathrm{A}^{n-} + \mathrm{H}^+ \overset{K_A}{\longleftrightarrow} \mathrm{Si-A}^{(n-1)-} + \mathrm{H_2O}. \quad (42)$$

and neglecting other types of complexation. For example, a divalent cation could, in principle, also make a complex with two $Si - O^-$ sites [*Davis et al.*, 1978].

Considering only the simple complexations of (41) and (42), the surface charge density Q_2 (equation (7)) becomes

$$Q_2 = \sum_x z_x \Gamma_{\mathrm{Si}-x}. \quad (43)$$

In Figure 19 the effect of changing the nature of the ion while keeping a fixed valence is studied for monovalent ions (Li^+, Na^+, K^+), and divalent ions (Mg^{2+}, Ca^{2+}, Ba^{2+}). In Figure 20, Na^+ and K^+ are compared when combined with Cl^- or NO_3^-. In Figure 19 the ζ potential for Na^+ is consistently smaller than for Li^+ and K^+, which are identical within the experimental accuracy. This effect is apparently not related to the actual ionic radius, as the size of the lithium ion is about half the size of the potassium ion [*Marcus*, 1988] or to the Stokes solvated radius which defines the ion mobility, as the mobilities of lithium and potassium are also different. For the divalent cations the observed ζ potentials are ordered according to ionic size, $\zeta(\mathrm{Mg}) > \zeta(\mathrm{Ca}) > \zeta(\mathrm{Ba})$.

In Figures 17 and 18 and in Table 1 it is possible to find values for the equilibrium constants so that the general features of the data are accommodated by the three-layer model, as indicated in the figure captions and in Table 1. However, the detailed variations of the chemical efficiency with the electrolyte resistivity do not agree well with the data (Figure 18),

Table 1. Streaming Potential Chemical Efficiencies E_S for Various Salts

Salt	E_S measured	E_S calculated ρ_f = 100 Ω m $pK_K = 4$, $pK_{Cl} = -9$
	Monovalent Ions	
NaCl	0.930 ± 0.003	0.933 ($pK_{Na} = 4$)
KNO_3	1.122 ± 0.004	1.12 ($pK_{NO_3} = -9.5$)
$NaNO_3$	0.995 ± 0.004	1.04 $pK_{Na} = 4$, $pK_{NO_3} = -9.5$
	Monovalent Cation With Divalent Anion	
K_2SO_4	0.937 ± 0.002	0.927 ($pK_{SO_4} = -7.5$)
Li_2CO_3	0.882 ± 0.003	0.88 ($pK_{Li} = 1.2$), $pK_{CO_3} = -7.4$
Na_2CO_3	0.836 ± 0.003	0.877 $pK_{Na} = 4$, $pK_{CO_3} = -7.4$
K_2CO_3	0.889 ± 0.003	0.893 ($pK_{CO_3} = -7.4$)
	Divalent Cation With Monovalent Anion	
$MgCl_2$	0.457 ± 0.003	0.43 ($pK_{Mg} = 5.1$)
$CaCl_2$	0.517 ± 0.002	0.525 ($pK_{Ca} = 5.1$)
$BaCl_2$	0.552 ± 0.002	0.56 ($pK_{Ba} = 5.3$)
	Divalent Ions	
$CaSO_4$	0.494 ± 0.003	0.577 $pK_{Ca} = 5.1$, $pK_{SO_4} = -7.5$
	Trivalent Cation	
$Tl(NO_3)_3$	0.377 ± 0.006	0.32 ($pK_{Tl} = 5.6$), $pK_{NO_3} = -9.5$

The reference is KCl. Most measurements are performed at pH = 5.7, except for the carbonates for which pH = 8. The experimental value is the average of the measurements from 40 to 2000 Ω m. The predictions of the three-layer EDL model correspond to the indicated values of the equilibrium constants and are given for an electrolyte resistivity of 100 Ω m. The equilibrium constants indicated in parentheses are chosen so that the prediction is matching the experimental value. When the equilibrium constants are not in parentheses, it means that the theoretical predictions is constrained by other measurements, and the comparison with the data is meaningful.

indicating that a more refined understanding of the surface chemistry is necessary.

Chemical efficiency depends in part on the mobility of the ions, which for the various ions imposes different ion concentrations for a given electrolyte resistivity. This effect is taken into account in our calculation and accounts for the observed difference between KCl and NaCl (see Table 1), at least at 100 Ω m.

Interestingly, the change of slope of ζ potential as a function of electrolyte resistivity observed for all other ions for electrolyte resistivity >1000 Ω m is not observed for carbonates (Figure 19). The carbonates show a linear variation over the whole range of resistivity up to the maximum value corresponding to pure distilled water. This may indicate that salt adsorption, taking place on the quartz surface, is affected by the presence of dissolved carbonate from the atmospheric CO_2. This effect would not be observed when the solution provides enough HCO_3^- ions from the salt.

Data for trivalent ions are presented in Figures 18 and 20. The chemical efficiency for Tl^{3+} is stable for electrolyte resistivity <2000 Ω m (Figure 18) and amounts to ~0.38 (Table 1), indicating that chemical efficiency seems to be close to the inverse of the valence of the cation. This empirical observation, however, is not supported by the three-layer model, in which the value of the chemical efficiency essentially results from the values of the adsorption constants and does not scale as $1/z_C$.

The ζ potential for Al^{3+} (Figure 20) decreases to almost zero for resistivities <1000 Ω m. The sharp decrease of the potential when small amounts of aluminum nitrate are added again points to the importance of additional chemical reactions taking place on the quartz surface, as already mentioned by *Morgan et al.* [1989] and *Ishido and Mizutani* [1981]. The presence of traces of Al^{3+} ions in the Fontainebleau samples may also explain the reduction of ζ potential with respect to predictions for high resistivity [*Rasmusson and Wall*, 1997; A. Revil, private communication, 1997]. Taking $pK_{A_1} = 3.7$, the prediction from the three-layer model is in good agreement with the data (Table 1 and Figure 20).

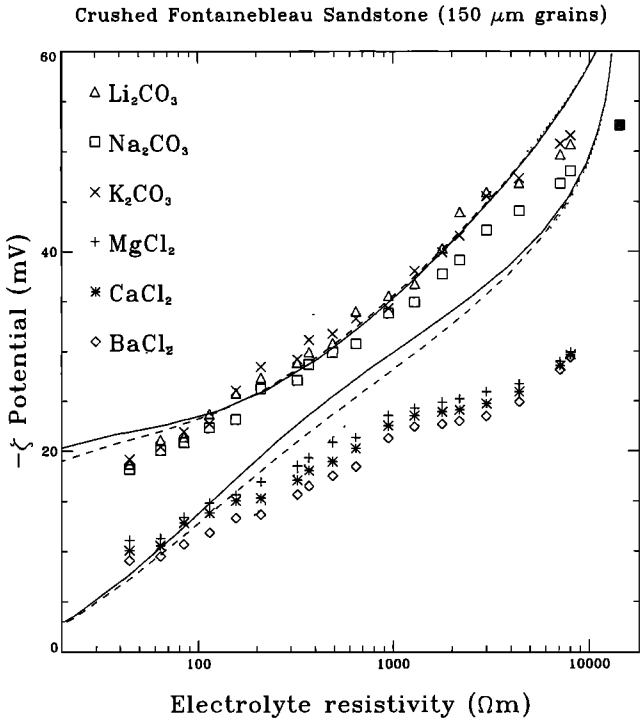

Figure 19. The ζ potential, inferred from streaming potential measurements using crushed Fontainebleau sandstone, as a function of electrolyte resistivity for several salt solutions with pH = 5.7 for chloride ions and pH varying between 7 and 8 for the carbonates. The results for several ions with the same valence but different natures are compared. The solid lines correspond to the predictions of the three-layer model [*Davis et al.*, 1978] for K_2CO_3 and $CaCl_2$. The dotted lines correspond to a pK_{cat} parameter increased by 1. The dashed lines correspond to a C_1 capacitance twice as large.

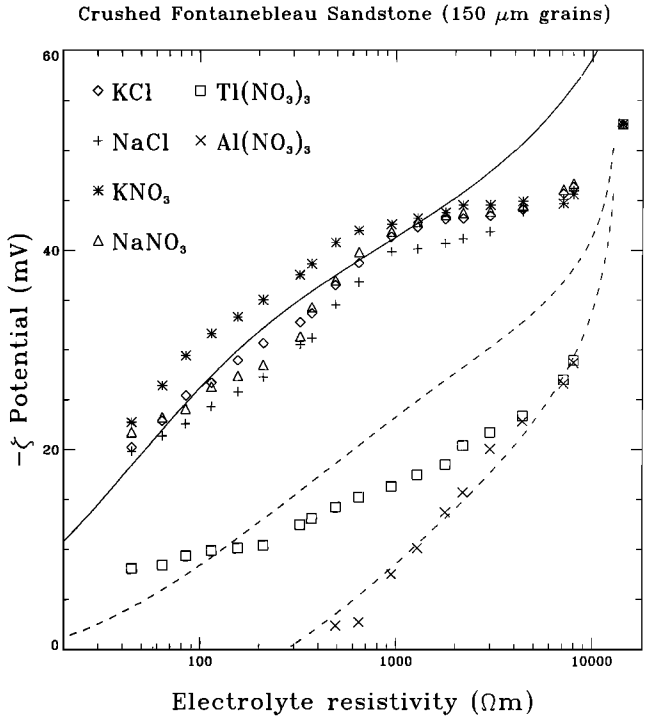

Figure 20. The ζ potential, inferred from streaming potential measurements using crushed Fontainebleau sandstone, as a function of electrolyte resistivity for several salt solutions with pH = 5.7. The results for Na^+ and K^+ are compared for two anions, and two examples of trivalent ions are given. The lines correspond to the predictions of the three-layer model [*Davis et al.*, 1978], from top to bottom KCl, $Tl(NO_3)_3$, and $Al(NO_3)_3$. The inferred values of the equilibrium constants are $pK_{Tl} = 5.6$ (Table 1) and $pK_{Al} = 3.7$.

4.5. Effect of Grain Size or Permeability

The inferred values of the ζ potential (using equation (33) and the experimental values of the streaming potentials) are shown in Figure 21 for several grain sizes as a function of the measured permeability. A variation of the ζ potential with permeability or grain size could be due to the presence of surface conductivity, as suggested by (33). The effect of typical pore size on the electrical structure of the EDL can be considered negligible [*Pride and Morgan*, 1991], as shown in the appendix.

In order to illustrate the role of the surface conductivity, two data sets are shown in Figure 21 with KCl, one for an electrolyte resistivity of 1000 Ω m and pH = 5.7 and one for an electrolyte resistivity of 400 Ω m and pH = 7. In order to be able to compare the two data sets the data set for 1000 Ω m

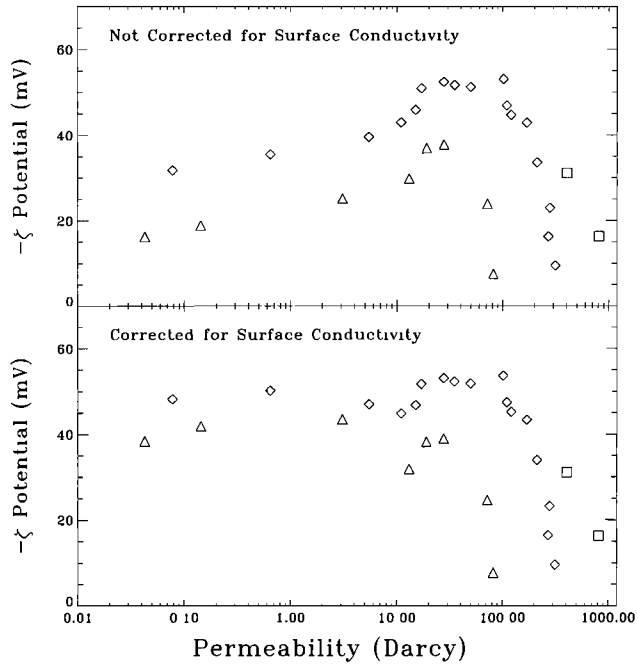

Figure 21a. The ζ potential, inferred from streaming potential measurements using crushed Fontainebleau sandstone, as a function of the sample permeability. The diamonds correspond to a KCl solution of 400 Ω m resistivity and pH = 7, and the triangles correspond to another crushed sample with a KCl solution of 1000 Ω m resistivity and pH = 5.7. The squares correspond to measurements with another experimental setup (see text). The results are compared with and without taking into account the effect of the surface conductivity on the streaming potential coefficient in equation (37).

and pH = 5.7 was transferred to the conditions of the data set with 400 Ω m and pH = 7 using the experimentally determined relations (37) and (40).

Smaller potentials are observed for permeability smaller than 5 darcies (grain sizes <150 μm). This reduction of ζ potential, which is more important for the data sample measured at ρ_f = 1000 Ω m, illustrates the fact that for smaller grain sizes the contribution of surface conductivity can not be neglected.

In Figure 21b our data show that a surface conductivity model of 0.17 mS/m at low permeability, 0.01 at high permeability and a smooth transition at 5 darcies, and a bulk formation factor F_0 which follow a scaling law $k^{-0.09}$, is consistent with the measurements. If the surface conductivity is thus taken into account using this model and (33), as in Figure 21a (bottom), the corrected ζ potential is roughly independent of the permeability for permeability <5 darcies. Also, measurements with different electrolyte resistivity agree, as the F/F_0 correction in (33) increases with increasing electrolyte resistivity.

For permeability larger than 50 darcies a sharp drop in streaming potential is observed in Figure 21a. To check the reproducibility of this observation, the ζ potential for two high values of permeability was measured using a different experimental setup in which the differential pressure across the sample was measured directly from the height of water in vertical glass tubes in order to be independent from head loss corrections. Although slightly higher than the other data, these two measurements confirm the drop at high permeability. A decrease of the streaming potential for large grain sizes was also noted by *Ahmad* [1964], although of smaller magnitude. For such large values of permeability, flow rate and turbulence effects might become important, although the deviation of the streaming coupling coefficient from linearity was not found to be large (Figure 4). For such flow rates, however, the size of the noncirculating electrolyte volumes in the sample may be of the order of magnitude of the grain size. More studies need to be performed to understand this effect, which may be important in some geophysical systems like fault zones. We expand further on the fact that the ζ potential is essentially constant between 10 mdarcy to 10 darcies in the companion paper by *Lorne et al.* [this issue].

5. Applications to Natural Geophysical Systems

5.1. Streaming Potentials for Various Rock Minerals

In order to extrapolate the results obtained in the laboratory to geophysical field conditions, the effects of different minerals and fluid chemistry must be addressed. Results of the measurement of the ζ potential for various crushed rocks are presented in Table 2. Rocks samples are crushed, and the grains are selected by sieving so that the resulting permeability in the experimental assembly is of the order of a few darcies at most. Crystalline and calcareous rocks are included, together with a sample of all major rock types present in a typical field site in the Alps, at the geological contact between the Belledone crystalline belt and the Mesozoic layers [*Perrier et al.*, 1998; *Trique et al.*, 1999].

For granite a ζ potential of -52 ± 1 mV is inferred for an electrolyte resistivity of 350 Ω m and pH = 7, compatible with results obtained for Westerly granite [*Morgan et al.*, 1989]. For most rocks the ζ potentials tend to be much smaller than the

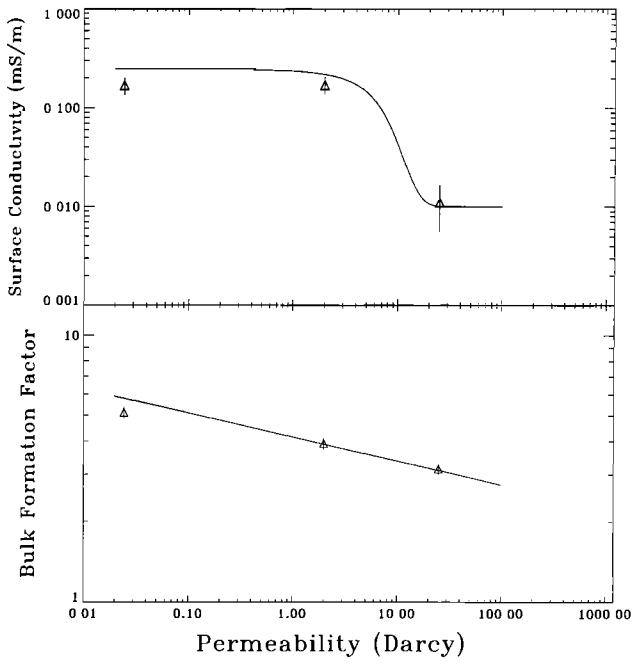

Figure 21b. Surface conductivity and bulk formation factor as a function of permeability. The three experimental measurements are compared with the ad hoc model (solid line) described in the text and used to correct for surface conductivity in Figure 21a.

Table 2. The ζ Potential for Various Rocks Measured With a Solution of KCl With pH = 5.7 for All Rocks Except for Limestones for Which the pH is 8

Rock	Mineralogy	Electrolyte Resistivity, Ω m	ζ Potential, mV
	Igneous and Metamorphic Rocks		
Granodiorite		350	−52 ± 1
Paragneiss (Alps)	clay/carbonate cement	312	−26 ± 0.5
Basalt (Pacific islands)	aluminosilicates	188	−18 ± 0.4
	Sedimentary Rocks With Quartz		
Fontainebleau sandstone	99% quartz	400	−40 ± 5
Vosges sandstone	quartz with hematite traces	80	−16 ± 0.3
Permian sandstone (Alps)	quartz + carbonates	300	−8.6 ± 0.2
Houiller sandstone (Alps)	quartz with anthracite and clay beds	400	−12 ± 0.2
Trias quartzite	quartz	400	−7.1 ± 0.1
Bajocian schist		295	−9.3 ± 0.2
	Carbonated Rocks		
Callovo-oxfordian limestone		311	−5 ± 0.2
Kimmeridgian limestone (Alps)	calcite with clay	300	−1.2 ± 0.2
Coral reef (Pacific island)	aragonite	200	−4.3 ± 0.2
Cellular dolomite (Alps)	dolomite	278	−4.2 ± 0.1

Electrolytes for limestones also include a significant content of dissolved carbonates. The indicated experimental errors correspond to the experimental error of a single measurement, except in the case of Fontainebleau sandstone where the sample to sample dispersion is taken into account.

results obtained for Fontainebleau sandstone. The results for several types of sandstone can be quite different. Increasing the number of mineral phases tends to reduce the ζ potential significantly. For limestones the electrolyte always contains a significant concentration of dissolved calcium and magnesium, which reduces the ζ potential as shown in section 4.

5.2. Streaming Potentials With Real Natural Water

Natural aqueous solutions are quite different from pure water with dissolved KCl, and the resistivity is rarely >400 Ω m, except for pure rain water (>1000 Ω m, although lower in industrial areas) and melted snow water in mountainous areas (for example, we measured about 1600 Ω m in the French Alps). In marine systems the resistivity of seawater is <0.2 Ω m (resistivity corresponding to the NaCl concentration at saturation) and the observation of streaming potentials in such environments is difficult. In a continental geophysical system, the resistivity of freshwater lakes varies around an average value of ~50 Ω m (value measured by the authors in lakes in the French Alps). For spring water the resistivity varies between 26 Ω m for a carbonate formation and 350 Ω m for a crystalline formation. The pH in general is close to 7 but can reach values as low as 6 for crystalline waters [*Probst et al.*, 1992] and as high as 8 for some carbonated waters [*Sigg et al.*, 1992].

The ζ potential was inferred for some mineral waters with one sample of crushed Fontainebleau sandstone from the measured streaming potentials using (33). The results are compiled in Table 3. The streaming potential chemical efficiency E_S has been calculated using (37) and (40).

The chemical efficiency is 0.44 ± 0.05 for the limestone water. This solution was obtained from crushed Kimmeridgian Garchy limestone at the edge of the Parisian basin. Its characteristics are similar to the parameters of a theoretical open calcite system in equilibrium with water and the atmosphere [*Sigg et al.*, 1992]. The ζ potential of this system increases with increasing pH (Figure 10), but the conductivity and the chemical efficiency are low. For a closed system, where pore water is not in contact with the atmosphere, the pH is high (pH = 9.9) and the concentrations of dissolved ions reduced; therefore the water resistivity is also higher.

Two measurements were performed with commercial mineral water. The St. Lambert water is one example of a naturally strongly carbonated water, but the measured chemical efficiency (Table 3) is high (0.8). This is in contradiction with the previous measurement with limestone water (E_S = 0.44 ± 0.05), suggesting that calcium carbonate has precipitated. The Volvic water is less conductive than the St. Lambert water and has a smaller dissolved carbonate content, a slightly higher ζ potential, and a similar chemical efficiency.

The chemical efficiency can also be calculated using the three-layer numerical model presented before. The values are given in Table 3 and are generally consistent with the measurements, except for the St. Lambert water and water typical of a crystalline environment [*Probst et al.*, 1992], which was not measured. This last example illustrates the higher resistivity of water in such areas. In conclusion, the chemical efficiency for mineral waters is ~80%, except for strongly carbonated waters for which it can be as low as 40%. In order to estimate the ζ potential in a given environment these efficiencies have to be applied to the values of the ζ potentials given in Table 2, according to the dominating mineralogy, and applying the scaling laws (37) and (40) for water resistivity and pH, respectively.

In order to estimate the streaming potential coefficient, the effect of the rock permeability must be understood, and this is the topic of the companion paper. The experimentally determined scaling laws can be used to estimate the streaming potential change that would be induced by a geochemical change. The relative potential variation δ_{12} that would be associated with a change of chemical conditions would be proportional to

$$\delta_{12} = \frac{(\rho_f)_2\zeta_2 - (\rho_f)_1\zeta_1}{(\rho_f)_1\zeta_1}, \tag{44}$$

where the subscript 1 refers to the initial conditions.

Table 3. The ζ Potential and the Streaming Potential Chemical Efficiencies E_S for Some Natural Waters Measured With Crushed Fontainebleau Sandstone

Electrolyte	pH	Electrolyte Resistivity, Ω m	ζ, mV	E_S	
				Measured	Calculated
KCl	5.5	390	−47	1	1
Calcite open system [*Sigg et al.*, 1992] $c_{HCO3-} = 0.907$ $c_{Ca2+} = 0.454$	8.3	(148)			(0.34)
Calcite closed system [*Sigg et al.*, 1992] $c_{HCO3-} = 0.081$ $c_{CO32-} = 0.033$ $c_{Ca2+} = 0.114$	9.9	(331)			(0.39)
Limestone solution (solution in equilibrium with Kimmeridgian limestone)	9.0	175	−20.2	0.44 ± 0.05	(0.34)
St. Lambert mineral water $c_{Ca2+} = 1.58$ $c_{Mg2+} = 0.31$ $c_{Na+} = 0.71$ $c_{K+} = 0.03$ $c_{Cl-} = 0.79$ $c_{SO42-} = 0.26$	7.2	24.6	−21.8	0.81 ± 0.08	(0.28)
Volvic mineral water $c_{Ca2+} = 0.22$ $c_{Mg2+} = 0.21$ $c_{Na+} = 0.44$ $c_{K+} = 0.15$ $c_{Cl-} = 0.34$ $c_{SO42-} = 0.08$	7.0	66	−26.0	0.77 ± 0.08	(0.59)
Vosges spring water [*Probst et al.*, 1992] $c_{Ca2+} = 0.19$ $c_{Mg2+} = 0.06$ $c_{Na+} = 0.08$ $c_{K+} = 0.02$ $c_{Cl-} = 0.06$ $c_{SO42-} = 0.21$	6.1	(125)			(0.58)

Calculated numbers in parentheses are obtained using the three-layer EDL numerical model. Concentrations are expressed in mmol/L.

For example, before the Kobe earthquake, geochemical changes were observed in the ground water [*Tsunogai and Wakita*, 1995]. In particular, an increase of 10% in the concentration of chloride ions, correlated to an increase of 30% of sulfate ions, was observed. A similar phenomenon was observed before an earthquake in the French Pyrénées [*Toutain et al.*, 1997]. Taking the typical composition of a water in a crystalline area given by *Probst et al.* [1992], one can estimate the δ_{12} factor as −10% for such a change of water chemistry, using the results from Table 3 and our three-layer numerical model. If we imagine a situation in which the electric potential is being monitored at two locations of an aquifer with a dipole length of 500 m or more, it is not unwarranted to expect to observe a static electric potential difference of ~100 mV at the bottom of piezometers, associated with the discharge flow of the aquifer. The above change in chemical conditions, without any change in the dynamics of the discharge, would produce an electrical signal of ~10 mV, which is larger than the drift noise of the electrodes and their installation schemes [*Perrier et al.*, 1997]. Such a slowly varying precursory electrical signal would then be observable in association with geochemical changes before earthquakes.

6. Conclusions

In this paper a systematic study of the ζ potential inferred from streaming potential measurements with crushed Fontainebleau sandstone is presented as a function of the electrolyte resistivity, pH, and ionic composition. The ζ potential was also inferred from streaming potential measurements using other rock types and natural groundwaters. The goal of these measurements is to improve our understanding of the physics of the electrical double layer. Various empirical laws were derived from the measurements which can be used for estimating streaming potential effects in geophysical systems, as illustrated by *Perrier et al.* [1998, 1999].

The results were compared with the predictions of a three-layer EDL numerical model [*Davis et al.*, 1978]. This model accounts for the general features of the data and allows values of the equilibrium constants of the adsorption reactions and the spatial structure of the EDL to be determined from the data. Variations of the ζ potential with pH can not be accounted for by a single-layer model but are generally predicted by the three-layer model; however, the details of the measured ζ potential variations as a function of electrolyte resistivity for

various types of ions are not well reproduced. More input from surface chemistry may be useful in assessing reasonable values for the parameters of the three-layer model. Also, the values of the equilibrium constants given in this paper are correlated with other parameters, and it may be hazardous to translate these values to other contexts. In any case, as illustrated by the comparisons presented in the figures, the data presented in this paper can be used to improve our theoretical understanding of the EDL.

Appendix

A1. Effect of Crack Size

The effect of a finite size crack can be studied by using a slight modification of (28). Indeed, the integration of the Poisson-Boltzmann equation (27) can be performed from 0 to a finite position d, where the derivative $d\varphi/dx = 0$ is 0. This is, for example, the case for a crack of half width d separating two parallel planar rock surfaces. The first-order differential equation for the potential is then, instead of (28),

$$\frac{d\varphi}{dx} = -\text{sign}\,(Q_S)\,\frac{v_0}{\chi_d} \cdot \sqrt{\frac{\sum_i c_i^0\left[\exp\left(-2z_i\frac{\varphi}{v_0}\right) - \exp\left(-2z_i\frac{\varphi_d}{v_0}\right)\right]}{2\sum_i z_i^2 c_i^0}}, \quad \text{(A1)}$$

where φ_d is the value of the potential in the center of the crack. Equation (A1), combined with the boundary condition (30), can be solved numerically, starting from some value of φ_d and iterating until the new boundary condition $d\varphi/dx = 0$ for $x = d$ is met within a preset precision. The results are shown in Figure A1 for a single-layer EDL model and a constant surface charge on the Stern plane. One can see that decreasing the aperture of a finite crack size increases the value of the Stern plane potential, and consequently the value of the ζ potential, for a fixed s parameter. However, this effect is very small, unless extremely small crack sizes are considered. The typical size of a pore in a Fontainebleau sandstone is ~150 μm, with throats of the order of 1 μm. The effect is larger for higher electrolyte resistivities, as illustrated in Figure A2a but remains very small. The finite size of cracks is neglected in our data interpretation.

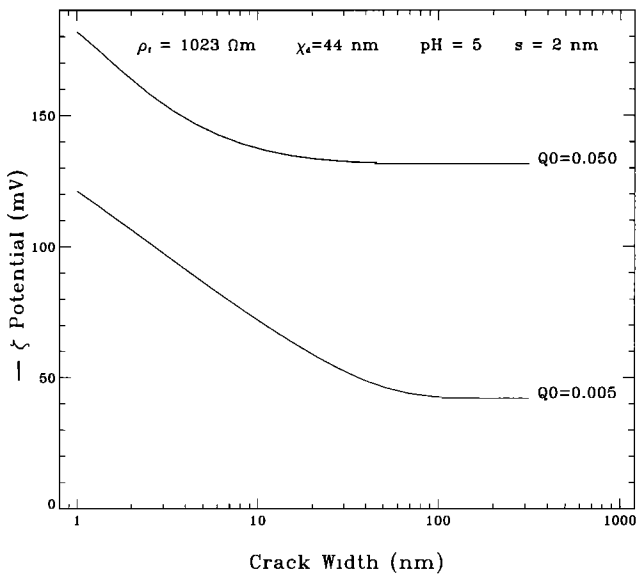

Figure A1. The ζ potential as a function of crack width, for a quartz-KCl solution interface, calculated using a simple one-layer model assuming a constant surface charge density on the Stern plane.

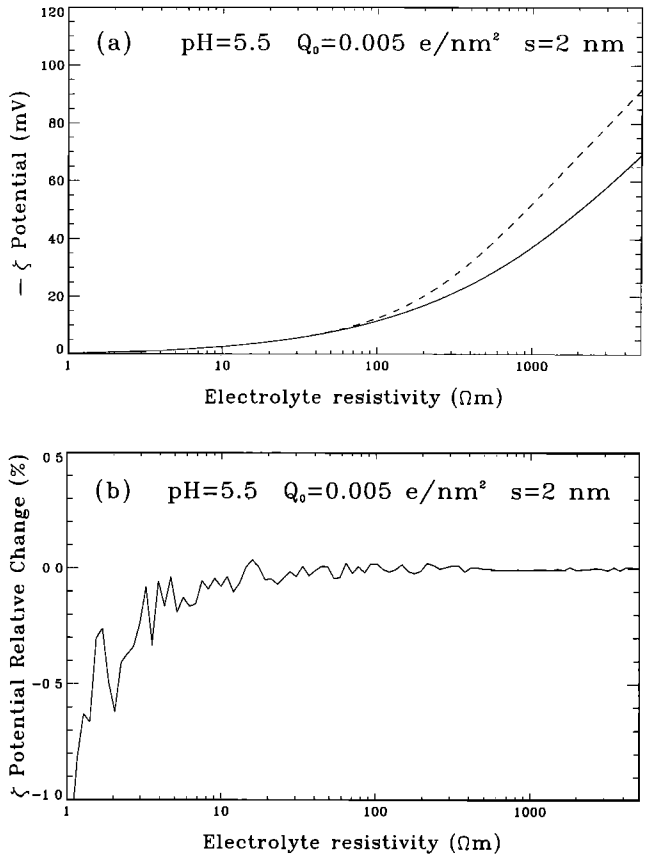

Figure A2. (a) The ζ potential as a function of electrolyte resistivity for an infinitely large crack (solid line) and a crack with a 20 nm half width (dotted line). (b) The effect on the ζ potential of including ion activity coefficients in the numerical integration of the Poisson-Boltzmann equation. The scatter of points reflects the accuracy of the numerical calculation.

A2. Effect of Ion-Ion Interactions

The interaction between ions can result in charge shielding for concentrated solutions. This may have a significant effect of the ζ potential, which is sensitive to the charge distribution of the ions. This effect was estimated using the Debye-Hückel theory of ionic activities [*Bard and Faulkner*, 1980]. Activity coefficients γ given by

$$\log\gamma = -0.509\sqrt{10^{-3}\,c_i^0\exp\left[-2z_i\frac{\varphi}{v_0}\right]}, \quad \text{(A2)}$$

were inserted in the Poisson-Boltzmann equation, which was then numerically integrated. In (A2) the effect is overestimated in order to take into account the fact that both cation and anion activities increase near the surface compared with the free electrolyte. The result is shown in Figure A2b. The calculated effect on the ζ potential is <1%. Ion-ion electro-

static interactions can therefore be neglected in our study even for electrolyte resistivities <10 Ω m. Ion-ion interactions do not explain the discrepancies between the data and some theoretical calculations.

Acknowledgments. The authors are grateful to the Laboratoire de Détection et de Géophysique for financial and technical support. Funds were also received from the French Ministry of Environment. Most of the experiments were performed with the help of Thierry Froidefond and Pierre Lalance. In addition, Jean Aupiais and his team of chemists helped with advise, equipment, measurements, and analysis of the electrolytes. Patrick Dupont is thanked for the fabrication of many pieces of the apparatus. The authors also acknowledge enlightening exchanges with Laurence Jouniaux, Jean-Pierre Pozzi, Paul Glover, and André Revil and especially thank Steve Pride for introducing them to the work of *Davis et al.* [1978]). M. Johnston and B. J. Wanamaker are thanked for their detailed and constructive review.

References

Ahmad, M. U., A laboratory study of streaming potentials, *Geophys. Prospect.*, *12*, 49–64, 1964.

Antraygues, P., and M. Aubert, Self potential generated by two-phase flow in a porous medium: Experimental study and volcanological applications, *J. Geophys. Res.*, *98*, 22,273–22,281, 1993.

Bard, A. J., and L. R. Faulkner, *Electrochemical Methods, Fundamentals and Applications*, John Wiley, New York, 1980.

Bernard, P., Plausibility of long distance electrotelluric precursors to earthquakes, *J. Geophys. Res.*, *97*, 17,531–17,546, 1992.

Bikerman, J. J., Electrokinetic potentials, in *The Encyclopedia of Electrochemistry*, edited by C. A. Hampel, pp. 471–475, Reinhold, New York, 1964.

Bogoslovsky, V. A., and A. A. Ogilvy, Natural potential anomalies as a quantitative index of the rate of seepage from water reservoirs, *Geophys. Prospect.*, *18*, 261–268, 1970.

Bogoslovsky, V. A., and A. A. Ogilvy, The study of streaming potentials on fissured media models, *Geophys. Prospect.*, *20*, 109–117, 1972.

Byerlee, J. D., Friction, overpressure and fault normal compression, *Geophys. Res. Lett.*, *17*, 2109–2112, 1990.

Chandler, R., Transient streaming potential measurements on fluid-saturated porous structures: An experimental verification of Biot's slow wave in the quasi-static limit, *J. Acoust. Soc. Am.*, *70*, 116–121, 1981.

Corwin, R. F., and D. B. Hoover, The self-potential method in geothermal exploration, *Geophysics*, *44*, 226–245, 1979.

David, C., Geometry of flow paths for fluid transport in rocks, *J. Geophys. Res.*, *98*, 12,267–12,278, 1993.

Davis, J. A., R. O. James, and J. O. Leckie, Surface ionization and complexation at the oxide/water interface, *J. Colloid Interface Sci.*, *63*, 480–499, 1978.

Ernstson, K., and H. U. Scherer, Self-potential variations with time and their relation to hydrogeologic and meteorological parameters, *Geophysics*, *51*, 1967–1977, 1986.

Fenoglio, M. A., M. J. S. Johnston, and J. D. Byerlee, Magnetic and electric fields associated with changes in high pore pressure in fault zones: Applications to the Loma Prieta ULF emissions, *J. Geophys. Res.*, *100*, 12,951–12,958, 1995.

Fujinawa, Y., T. Kumagai, and K. Takahashi, A study of anomalous underground electric field variations associated with a volcanic eruption, *Geophys. Res. Lett.*, *19*, 9–12, 1992.

Glover, P. W. J., P. G. Meredith, P. R. Sammonds, and S. A. F. Murell, Ionic surface conductivity in sandstone, *J. Geophys. Res.*, *99*, 21,635–21,650, 1994.

Hashimoto, T., and Y. Tanaka, A large self-potential anomaly on Unzen volcano, Shimabara peninsula, Kyushu island, Japan, *Geophys. Res. Lett.*, *22*, 191–194, 1995.

Iler, R. K., *The Chemistry of Silica*, John Wiley, New York, 1979.

Ishido, T., and H. Mizutani, Experimental and theoretical basis of electrokinetic phenomena in rock-water systems and its applications to geophysics, *J. Geophys. Res.*, *86*, 1763–1775, 1981.

Johnson, P. A., and T. V. McEvilly, Parkfield seismicity: Fluid-driven?, *J. Geophys. Res.*, *100*, 12,937–12,950, 1995.

Jouniaux, L., and J. P. Pozzi, Permeability dependence of streaming potential in rocks for various fluid conductivities, *Geophys. Res. Lett.*, *22*, 485–488, 1995a.

Jouniaux, L., and J. P. Pozzi, Streaming potential and permeability of saturated sandstones under triaxial stress: Consequences for electrotelluric anomalies prior to earthquakes, *J. Geophys. Res.*, *100*, 10,197–10,209, 1995b.

Jouniaux, L., and J. P. Pozzi, Laboratory measurements anomalous 0.1–0.5 Hz streaming potential under geochemical changes: Implications for electrotelluric precursors to earthquakes, *J. Geophys. Res.*, *102*, 15,335–15,343, 1997.

Lorne, B., F. Perrier, and J. P. Avouac, Streaming potential measurements, 2, Relationship between electrical and hydraulic flow patterns from rock samples during deformation, *J. Geophys. Res.*, this issue.

Malengreau, B., J. F. Lénat, and A. Bonneville, Cartography and temporal observation of self-potential (SP) anomalies at Piton de la Fournaise, *Bull. Soc. Géol. Fr.*, *165*, 221–232, 1994.

Marcus, Y., Ionic radii in aqueous solutions, *Chem. Rev.*, *88*, 1475–1498, 1988.

Massenet, F., and V. N. Pham, Mapping and surveillance of active fissure zones on a volcano by the self-potential method, Etna, Sicily, *J. Volcanol. Geotherm. Res.*, *24*, 315–338, 1985a.

Massenet, F., and V. N. Pham, Experimental and theoretical basis of self-potential phenomena in volcanic areas with reference to results obtained on Mount Etna (Sicily), *Earth Planet. Sci. Lett.*, *73*, 415–429, 1985b.

Michel, S., and J. Zlotnicki, Self-potential and magnetic surveying of La Fournaise volcano (Réunion Island): Correlations with faulting, fluid circulation, and eruption, *J. Geophys. Res.*, *103*, 17,845–17,857, 1998.

Mizutani, H., T. Ishido, T. Yokotura, and S. Ohnishi, Electrokinetic phenomena associated with earthquakes, *Geophys. Res. Lett.*, *3*, 365–368, 1976.

Morat, P., and J. L. Le Mouël, Electrical signals generated by the collapse of the pillars of a gypsum quarry, *C. R. Acad. Sci., Ser. II*, *308*, 33–38, 1989.

Morat, P., and J. L. Le Mouël, Electrical signals generated by stress variations in porous non saturated rocks, *C. R. Acad. Sci., Ser. II*, *315*, 955–963, 1992.

Morgan, F. D., E. R. Williams, and T. R. Madden, Streaming potential properties of Westerly granite with applications, *J. Geophys. Res.*, *94*, 12,449–12,461, 1989.

Muir-Wood, R., and G. C. P. King, Hydrological signatures of earthquake strain, *J. Geophys. Res.*, *98*, 22,035–22,068, 1993.

Nur, A., and J. R. Booker, Aftershocks caused by fluid flow, *Science*, *175*, 885–887, 1972.

Ogilvy, A. A., M. A. Ayed, and V. A. Bogoslovsky, Geophysical studies of water leakages from reservoirs, *Geophys. Prospect.*, *17*, 36–62, 1969.

Overbeek, J. T., *Colloid Science*, edited by H. R. Kruyt, Elsevier, New York, 1960.

Park, S. K., M. J. S. Johnston, T. R. Madden, and H. F. Morrison, Electromagnetic precursors to earthquakes in the ULF band: A review of observations and mechanisms, *Rev. Geophys.*, *31*, 117–132, 1993.

Perrier, F., et al., A one-year systematic study of electrodes for long period measurement of the electric field in geophysical environments, *J. Geomagn. Geoelectr.*, *49*, 1677–1696, 1997.

Perrier, F., M. Trique, B. Lorne, J. P. Avouac, S. Hautot, and P. Tarits, Electric potential variations associated with lake level variations, *Geophys. Res. Lett.*, *25*, 1955–1958, 1998.

Perrier, F., M. Trique, J. Aupiais, U. Gautam, and P. Shrestha, Electric potential variations associated with periodic spring discharge in western Nepal, *C. R. Acad. Sci., Ser. II*, *328*, 73–79, 1999.

Pisarenko, D., P. Morat, and J. L. Le Mouël, On a possible mechanism of sandstone alteration: Evidence from electric potential measurements, *C. R. Acad. Sci., Ser. II*, *322*, 17–24, 1996.

Pride, S., Governing equations for the coupled electromagnetics and acoustics of porous media, *Phys. Rev. B Condens. Matter*, *50*, 15,678–15,696, 1994.

Pride, S. R., and F. D. Morgan, Electrokinetic dissipation induced by seismic waves, *Geophysics*, *56*, 914–925, 1991.

Probst, A., D. Viville, B. Fritz, B. Ambroise, and E. Dambrine, Hydrochemical budgets of a small forested granitic catchment exposed to acid deposition: The Strengbach catchment case study (Vosges massif, France), *Water Air Soil Pollut.*, *62*, 337–347, 1992.

Rasmusson, M., and S. Wall, Electrostatic characterisation of Al-modified, nanosized silica particles, *Colloids Surf. A*, *122*, 169–181, 1997.

Revil, A., and P. W. J. Glover, Theory of ionic-surface electrical conduction in porous media, *Phys. Rev. B Condens. Matter*, *55*, 1757–1773, 1997.

Ruffet, C., Y. Gueguen, and M. Darot, Complex conductivity measurements and fractal nature of porosity, *Geophysics*, *56*, 758–768, 1991.

Scholz, C. H., L. R. Sykes, and Y. P. Aggarwal, Earthquake prediction: A physical basis, *Science*, *181*, 803–810, 1973.

Sigg, L., W. Stumm, and P. Behra, *Chimie des Milieux Aquatiques*, Masson, Paris, 1992.

Sleep, N. H., and M. L. Blanpied, Creep, compaction and the weak rheology of major faults, *Nature*, *359*, 687–692, 1992.

Somasundaran, P., and R. D. Kulkarni, A new streaming potential apparatus and study of temperature effects using it, *J. Colloid Interface Sci.*, *45*, 591–600, 1973.

Sprunt, E. S., T. B. Mercer, and N. F. Djabbarah, Streaming potential from multiphase flow, *Geophysics*, *59*, 707–711, 1994.

Toutain, J. P., M. Munoz, F. Poitrasson, and A. C. Lienard, Spring-water chloride ion anomaly prior to an $ML = 5.2$ Pyrenean earthquake, *Earth Planet. Sci. Lett.*, *149*, 113–119, 1997.

Trique, M., P. Richon, F. Perrier, J. P. Avouac, and J. C. Sabroux, Radon emanation and electric potential variations associated with transient deformation in the vicinity of reservoir lakes, *Nature*, *399*, 137–141, 1999.

Tsunogai, U., and H. Wakita, Precursory chemical changes in ground water: Kobe earthquake, Japan, *Science*, *269*, 61–63, 1995.

Wurmstich, B., and F. D. Morgan, Modeling of streaming potential responses caused by oil well pumping, *Geophysics*, *59*, 46–56, 1994.

Yoshida, S., M. Uyeshima, and M. Nakatani, Electric potential changes associated with slip failure of granite: Preseismic and coseismic signals, *J. Geophys. Res.*, *102*, 14,883–14,897, 1997.

Zlotnicki, J., and J. L. Le Mouël, Volcanomagnetic effects observed on Piton de la Fournaise volcano (Réunion Island): 1985–1987, *J. Geophys. Res.*, *93*, 9157–9171, 1988.

Zlotnicki, J., and J. L. Le Mouël, Possible electrokinetic origin of large magnetic variations at La Fournaise Volcanoe, *Nature*, *343*, 633–636, 1990.

Zlotnicki, J., S. Michel, and C. Annen, Anomalies de polarisation spontanée et systèmes convectifs sur le volcan du Piton de la Fournaise (Ile de la Réunion, France), *C. R. Acad. Sci., Ser. II*, *318*, 1325–1331, 1994.

Zohdy, A. A. R., L. A. Anderson, and L. J. P. Muffler, Resistivity, self-potential, and induced-polarization surveys of a vapor-dominated geothermal system, *Geophysics*, *38*, 1130–1144, 1973.

J.-P. Avouac, B. Lorne, and F. Perrier, Commissariat à l'Énergie Atomique, Laboratoire de Détection et de Géophysique, BP12, F-91680 Bruyères-le-Châtel, France. (perrier@ldg.bruyeres.cea.fr)

(Received April 3, 1998; revised March 26, 1999;
accepted April 20, 1999.)